MONASH University

Monitoring of Crack Propagation in Fibre-Reinforced-Polymer (FRP) Strengthened Steel Plates Using Guided Waves

Yikuan Wang

Bachelor of Engineering (Honours)

A thesis submitted for the degree of *Master of Engineering Science (Research)* at Monash University in 2016

Faculty of Engineering

8th April, 2016

Copyright notice

Abstract

The application of Lamb waves to monitor fatigue crack propagation and to detect fatigue crack initiation in carbon fibre reinforced polymer (CFRP) strengthened steel plates is investigated. A literature review of recent developments and advances of Lamb wave-based structural health monitoring (SHM) applications is presented. The characteristics of Lamb waves, current signal processing and feature extraction technique, and damage-detection techniques are studied. The mechanism of nonlinear Lamb waves, especially contact acoustic nonlinearity (CAN), is investigated, along with latest numerical and experimental achievements and findings of nonlinear Lamb wave-based SHM.

This study consists of two parts, monitoring fatigue crack propagation and detecting crack initiation. Two methods are proposed accordingly. The first uses linear Lamb waves to monitor the fatigue crack propagation. 3-dimensional Finite element (FE) models are developed in Abaqus to assess the proposed linear method, along with Lab-based experimental validation. Based on the results, it is concluded that Lamb waves are sensitive to the concealed fatigue cracks, and Lamb wave-based SHM is a promising technique to monitor fatigue crack propagation.

The second method employs nonlinear Lamb waves to detect the initiation of fatigue crack because of their remarkable sensitivity to small-scale damage. The principles of wave nonlinearity are presented and the mechanics of CAN is discussed. The proposed nonlinear method is first assessed in steel plates. The effects of CFRP laminates on Lamb waves are investigated and the signals

captured in steel plates with/without CFRP laminates are compared. The simulation and experimental results are presented and discussed.

Declaration

This thesis contains no material which has been accepted for the award of any other degree or diploma at any university or equivalent institution and I affirm that, to the best of my knowledge and belief, this thesis contains no material previously published or written by another person, except where due reference is made in the text of the thesis.

Yikuan Wang

Department of Civil Engineering

Monash University

April, 2016

To my beloved parents

Acknowledgement

I am sincere grateful to my supervisor, Dr. Ye Lu, for his invaluable guidance, for his patience and for his continuous support during my Master candidature at Monash University. The door to Dr. Ye Lu's office was always open whenever I had problems about my research. I also wish to express my sincere gratitude to my co-supervisor, A/Prof. Wenhui Duan for his guidance and experiences that have ensured my research progress.

I wish to thanks all lab staffs for their assistance in performing experiments at the Civil Engineering Lab. Special thanks go to Mr. Long Goh and Mr. Mark Tayler for their exceptional assistance in ordering all necessary material, set-up and operating equipments.

I wish to thank all staff members in Department of Civil Engineering in Monash University, especially Mrs. Jenny Manson, who has provided invaluable support and assistance during my candidature.

I would also like to express my gratitude to all my office mates, Zhenhan Wang, Bing Fan, Li Chik, Qianhui Zhang, Tim Werner, Zhujing Zhang, Feng Lin and Xue Le. Thanks for all the wonderful time we had together.

I am grateful to those who provided financial support to this project. My scholarships were Monash Graduate Scholarship (MGS) funded by Monash University and Faculty of Engineering International Postgraduate Research Scholarship (FEIPRS) provided by Faculty of Engineering, Monash University.

Last but not the least, I would like to express my heartfelt gratitude to all my friends for their encouragement and support and especially my parents, Yumei Li and Yujun Wang, for their unconditional love.

This work is dedicated to my parents.

Yikuan Wang

April, 2016

Table of Contents

Copyright notice i
Abstract ii
Declaration iv
Acknowledgement vi
Notations III
List of Tables V
List of Figures VI
Chapter 1. Introduction 1
1.1. Motivation 1
1.2. Thesis outlines 2
Chapter 2. Literature review 4
2.1. Generation of Lamb waves 4
2.2. Signal processing and feature extraction 7
2.3. Data Fusion 9
2.5. Research gap and research aim 14
2.6. Summary 17
Chapter 3. Methodology 18
3.1. Specimen 18
3.1.1. Specimen configuration 18
3.1.2. Material properties 19
3.2. Selection of wave mode, waveform and excitation frequency 20
3.3. De-noising of signal 22
3.4. Damage detection strategy 23
3.5. Numerical method 26
3.5.1. Mesh convergence 27
3.5.2. Signal actuation and acquisition 29
3.5.3. Modelling of damage 30
3.6. Experimental methods 31
3.6.1. Specimen preparation 31
3.6.2. Test set-up 32
3.7. Summary 35
Chapter 4. Monitoring fatigue crack propagation using linear Lamb waves 36

4.1. Excitation frequency 36
4.2. Model analysis 37
4.2.1. Simulation results 41
4.3. Experimental analysis 44
4.3.1. De-noising of raw signals 45
4.3.2. Experiment results 49
4.4. Summary 52
Chapter 5. Identification of crack initiation using nonlinear Lamb waves 54
5.1. Excitation frequency 54
5.2. Numerical modelling analysis 55
5.2.1. Feature extraction and damage identification 56
5.2.2. Wave-damage interaction when specimen subjected to a constant tensile loading 60
5.2.3. Wave-damage interaction in CFRP-strengthened steel plates 63
5.3. Experimental analysis 67
5.3.1. Measurements of fatigue crack size 68
5.3.2. Experimental results 70
5.4. Summary 76
Chapter 6. Conclusions and recommendations 78
6.1. Conclusion 78
6.2. Recommendation for future work 81
References 83
Appendix 88

Notations

The abbreviations frequently used in this thesis are listed below with corresponding definitions.

A_0	fundamental anti-symmetrical mode
CAN	contact acoustic nonlinearity
CFRP	carbon fibre reinforced polymer
CWT	continuous wavelet transform
DI	Damage index
DSF	Digital signal filter
DWT	discrete wavelet transform
FE	Finite element
FFT	Fast Fourier transform
FSWT	frequency slice wavelet transform
GW	guided waves
LRS	linear response subtraction
MRD	minimum resolvable distance
PSD	Power-spectral-density
RMS	root mean square
S_0	fundamental symmetrical mode
SD	synchronous demodulation
SHM	Structural health monitoring
SNR	signal-to noise ratio
STFT	short-time Fourier transform
PDI	probabilistic-based diagnostic imaging
PZT	Lead zirconate titanate
TCR	transmission coefficient ratio
ToF	Time of flight

WT	wavelet transform

The symbols used in this thesis are listed below with corresponding definitions.

$D_{a,l}$	Distance from actuator to damage
$D_{i,s}$	Distance from damage to sensor
f_0	Excitation frequency
f_{min}	Minimum of frequency range
f_{max}	Maximum of frequency range
v_0	Group velocity at the central frequency
v_{min}	Maximum velocities in the wave packet
v_{max}	Maximum velocities in the wave packet

List of Tables

Table 3-1 Measured material properties of steel and CFRP plates.....20
Table 4-1 Engineering constants for CFRP 38
Table 4-2 Comparison of velocities of Lamb wave travelling in steel plate and CFRP-strengthened steel plate 41
Table 4-3 Comparison of velocities of Lamb wave travelling in steel plate and CFRP strengthened steel plate calculated using DISPERSE, FE model and experiment.....49

List of Figures

Figure 2-1 Schematic diagram illustrating CAN [52, 57] 13
Figure 3-1 Specimen geometry and configuration (a) Steel plate with through-thickness hole and crack (b) CFRP strengthened steel plate (c) Layout of PZT sensors 19
Figure 3-2 a) Phase and b) group velocity for a 10mm thick steel plate calculated using DISPERSE® 21
Figure 3-3 a) 5.5-cycle and b) 15.5-cycle Hanning-windowed tone burst 22
Figure 3-4 Principle of DWT-based signal decomposition 23
Figure 3-5 Wave paths for reflected signal and diffracted signal 24
Figure 3-6 The illustration of relative distance 24
Figure 3-7 Principle of damage triangulation 25
Figure 3-8 Finite element model in ABAQUS a) Top view of steel plate b) Side view of steel plate c) modelling of a PZT d) modelling of damage e) Top view of CFRP strengthened steel plate and f) Side view of CFRP strengthened steel plate 28
Figure 3-9 PZT model and forces 29
Figure 3-10 Simulation of Lamb waves propagating from the PZT model 30
Figure 3-11 "seam" cracks to enable CAN 31
Figure 3-12 Steel plate and CFRP strengthened steel plate with surface-mounted PZT sensors 32
Figure 3-13 Fatigue test procedure 34
Figure 3-14 Data acquisition procedure 34
Figure 3-15 Test set-up 35
Figure 4-1 Maximum amplitude of the signals against frequencies 37
Figure 4-2 Diagram of CFRP-strengthened steel plate with surface mounted PZTs 38
Figure 4-3 Simulation of damage a) benchmark state b) crack state (2mm), and c) crack state (15mm) 39
Figure 4-4 Sample waveforms captured in sensing path S1-S5 and S2-S4 40
Figure 4-5 Calculated crack lengths (FE) for sensing path a) S1-S5, b) S1-S6, c) S2-S4, d) S2-S5, and e) S2-S6 43
Figure 4-6 Calculated crack length (FE) based on all sensing path within the sensor network 44
Figure 4-7 Beach marks on failure face of the specimen 45
Figure 4-8 Captured signal in path S1-S5 a) original signals, and b) de-noised signals 47
Figure 4-9 Frequency profile of typical signal of damage state 48
Figure 4-10 Decomposition of raw signal using MATLAB 48
Figure 4-11 Raw signal vs. de-noised signal 49
Figure 4-12 Calculated crack lengths (Test 1) for sensing path a) S1-S4, b) S1-S5, c) S1-S6, d) S2-S5, e) S2-S6, f) S3-S4, and G) S3-S5 51

Figure 4-13 Calculated crack length (Experiment) based on all sensing paths within the sensor network 52
Figure 5-1 (a) Typical benchmark and damage state signals in the time domain (captured via S2-S4) and (b) FFT of the benchmark and current state signal 57
Figure 5-2 Filter design in MATLAB 57
Figure 5-3 (a) the amplitude profiles at the fundamental frequency, where S1 mode is the first arrival mode at time t1 and (b) the amplitude profiles at the double frequency, where damage-induced nonlinearity arrives at t2. 58
Figure 5-4 an image showing the probability of damage detected via S2-S4 sensing path 59
Figure 5-5 Diagnostic image after fusion (a) addition result and (b) product result 60
Figure 5-6 Simulation of tensile loading applied on specimen 61
Figure 5-7 Deformed model in which the fatigue crack is in open scenario under tensile loading 61
Figure 5-8 Illustration of importing deformed configuration into Abaqus 62
Figure 5-9 Amplitude profiles of loaded signal and unloaded at (a) fundamental frequency and (b) double frequency 63
Figure 5-10 Amplitude profile of loaded signal and benchmark signal at (a) fundamental frequency and (b) double frequency 63
Figure 5-11 CFRP strengthened steel plate model 64
Figure 5-12 CFRP-steel constraint in Abaqus 65
Figure 5-13 Typical benchmark signals captured in steel plate and CFRP strengthened steel plate via sensing path S2-S4 (a) waveform in time-domain and (b) amplitude profile in time-domain. 66
Figure 5-14 (a) Benchmark and damage signals in steel and CFRP strengthened steel plate via sensing path S2-S4, and (b) zoom-in of Figure 5-14 (a) 67
Figure 5-15 (a) Steel plate specimen with 10 surface-mounted PZT sensors and (b) configuration of steel plate 68
Figure 5-16 a) configuration of CPC03 crack propagation gauge b) CPC03 crack propagation gauge and crack propagation direction. 69
Figure 5-17 Crack propagation gauge bonded to the specimen surface 69
Figure 5-18 Crack on crack propagation gauge 70
Figure 5-19 Benchmark and crack signal captured in path S1-S6 in (a) time-domain and (b) frequency domain 72
Figure 5-20 Benchmark and cracked signal at double frequency in time domain 72
Figure 5-21 Energy profiles of benchmark and cracked signals at double frequency captured via sensing path (a) S1-S6, (b) S2-S7, (c) S3-S8, (d) S4-S9, and (e) S5-S10. 74
Figure 5-22 energy profile of crack signals at double frequency captured in sensing path S1-S6, S2-S7, and S3-S8 75

Figure 5-23 (a) captured benchmark and cracked signal in time domain via S2-S5 and (b) energy profile of benchmark and cracked signal at double frequency 76

Chapter 1. Introduction

1.1. Motivation

There are a large number of steel structures, such as bridges, pipelines, building frames and mining equipments that are subject to fatigue loading and degradation of ageing metallic structure elements due to fatigue loading can lead to integrity failure of civil infrastructure. In many cases, degradation occurs only at the critical locations of certain parts of the structure, and it would be more economical and convenient to retrofit those parts rather than replace the entire structure. The bonding of CFRP materials to strengthen ageing steel structures has attracted considerable attention from researchers seeking to extend the service life of ageing steel structures by harnessing the outstanding properties of CFRP such as high modulus, high strength-to-weight ratio and excellent resistance to environmental degradation [1].

To ensure the functionality and integrity of retrofitted structures, long-term monitoring of structural integrity is required. However, with the bonding of CFRP materials, concealed crack growth due to fatigue loading cannot be detected by common inspection methods. As an alternative, Lamb wave-based structural health monitoring (SHM) techniques have been successfully applied by researchers to locate and quantify defects in plate-like metallic structures The use of Lamb waves for SHM has the following advantages: (1) capability of propagation over a long distance with low attenuation and low energy consumption, (2) sensitivity to both surface and through-thickness damage, (3) high sensitivity to minor damage, and (4) ability to continuously monitor with low cost and labour requirement, which make it a promising technique for long-

term online monitoring of the retrofitted structures. For implementing this technique in CFRP-strengthened steel plates, it is crucial to investigate the wave propagation characteristics in the retrofitted zone and to determine the feasibility of applying this technique to monitor crack growth in the strengthened steel plates.

1.2. Thesis outlines

This thesis consists of 6 chapters. The motivation of this research project, research aims, research objectives and the contents of each chapter are introduced in Chapter 1.

Chapter 2 gives a brief review of recent developments and advances of Lamb wave-based SHM applications. The principles of Lamb waves are briefly introduced, followed by the review of feature extraction and signal processing techniques. The pattern recognition technologies are outlined and compared. The basic principles of nonlinear ultrasonic phenomena are reviewed and the process of nonlinear ultrasonic techniques is presented, along with the review of previous numerical and experimental studies on nonlinear Lamb wave-based structural health monitoring. These reviews not only provide a comprehensive understanding of the current progress in the field of Lamb wave-based SHM, but also identify the research gaps in this study.

Chapter 3 presents the proposed methodologies for Lamb wave-based SHM to monitor fatigue crack propagation and to detect fatigue crack initiation. The specimen is designed and the configuration and the material properties are summarised. The selection of wave modes, waveform and the excitation

frequency, and the damage detection strategy is discussed. The modelling method and experiment set-up are also presented.

Chapter 4 examines the effectiveness of using linear Lamb waves to monitor fatigue crack propagation in CFRP-strengthened steel plates. The numerical and experimental results are presented and discussed.

Chapter 5 assesses the effectiveness of using nonlinear Lamb wave-based method to identify crack initiation. First, a 3-dimensional steel plate is modelled to exam the proposed method. Then the signals captured in steel plates with and without surface-mounted CFRP laminates are compared. Experiments are conducted on both steel plates and CFRP-strengthened steel plates. The numerical and experimental results are presented and discussed.

Chapter 6 highlights the conclusions in this thesis and recommendations for future works.

Chapter 2. Literature review

Lamb waves, one of guided waves (GW), are elastic waves which propagate in plate-like structures and are guided by the upper and lower surfaces of a structure. Taking advantages of its capability of propagating over a significant distance and high sensitivity to abnormalities in or near the wave propagation path, Lamb waves are widely employed to detect damage and evaluate integrity of a board range of aerospace, civil and mechanical engineering infrastructures. Early developments and researches of applying GW in structural health monitoring are well documented in [2-4]. This chapter mainly presented the literature review of the recent developments and advances of GW based SHM techniques. The generation method of Lamb waves was briefly introduced, followed by the review of feature extraction and signal processing techniques. The pattern recognition techniques were discussed and compared. The overall progress of nonlinear ultrasonic techniques was discussed with a brief review of basic principle of nonlinear ultrasonic phenomena. Lastly, previous studies, both numerical and experimental, of nonlinear ultrasonic wave based non-destructive evaluation were reviewed.

2.1. Generation of Lamb waves

Four crucial components, i.e. transducer, wave mode, wave frequency, and waveform, are required to generate Lamb waves. Transducers are grouped into four categories, ultrasonic probes, laser, piezoelectric elements, and interdigital transducers, among which piezoelectric elements are widely accepted as surface-mounted transducers for in situ structural health monitoring by researchers [5-9] for its excellent performance in Lamb wave generation and acquisition as well as wide frequency responses with low power consumption,

negligible weight and volume, excellent integration into host structure with minimum intrusion, and low cost [3, 4].

A desirable diagnostic Lamb wave mode should feature (1) less-dispersion; (2) low attenuation; (3) high sensitivity to damage; (4) easy excitability; and (5) good detectability [3, 4, 10]. The bandwidth, cycle number, frequency and magnitude of a wave mode are crucial factors that can enhance the capability of damage detection upon selecting the diagnostic wave. Various Lamb wave modes at different frequencies in plates were examined [10], and it is concluded that a narrow bandwidth signal with a certain number of cycles can greatly prevent wave dispersion. For this reason, windowed tonebursts are used to narrow the bandwidth of selected Lamb wave modes. The most widely adopted window function is the Hanning *h(n)*, defined as:

$$h(n) = \frac{1}{2}\left[1 - \cos\left(\frac{2\pi n}{N-1}\right)\right], \quad (n = 1,2,\dots,N) \qquad [2.1]$$

Where N is the sampling points.

The relationship between the frequency range [f_{min}, f_{max}], toneburst cycle number n, and excitation frequency f_0 is defined as:

$$f_{min} = f_0 \times \left(1 - \frac{k}{n}\right), \qquad [2.2a]$$

$$f_{max} = f_0 \times \left(1 + \frac{k}{n}\right), \qquad [2.2b]$$

Where k is a constant depending on the bandwidth. Equation 2.2 indicates that, as the cycles number increases, the wave bandwidth is reduced, the signal energy is more concentrated around the central excitation frequency and the peak amplitude increases, and thereby wave dispersion is reduced [11].

However, a large cycle number may result in overlapping in the time domain among the different wave components which propagate at different velocities. A trade-off between the cycle number and its duration must be considered for each case. The most suitable cycle number and frequency of the selected Lamb wave modes can be determined using minimum resolvable distance (MRD), defined as [4]:

$$MRD = \frac{v_0}{d}\left[l \times \left(\frac{1}{v_{min}} - \frac{1}{v_{max}}\right) + T_{initial}\right]\Big|_{min}, \qquad [2.3]$$

Where *l* and *d* are the wave propagation distance and plate thickness; v_0, v_{min}, and v_{max} are the group velocity at the central frequency, minimum and maximum velocities in the wave packet to travel through the distance of *l*; $T_{initial}$ is the initial time duration of the wave packet. It was indicated that the smaller a MRD value, the better resolution, and the more suitable the frequency and cycle number for the diagnostic signal [4].

The fundamental symmetrical mode, S0 and anti-symmetrical mode, A0 have been found to have very low MRDs, and thereby are commonly used for damage detection. The S0 mode features lower attenuation, faster propagation velocity and lower dispersion in the low frequency range, whereas A0 mode outperforms S0 mode with shorter wavelength, larger signal amplitude at certain frequencies and easier means of activation[3, 4]. It is concluded that S0 mode is more sensitive to defects in the structural thickness [12-14], while A0 mode exhibits higher sensitivity to surface damage [15, 16] such as surface cracks, corrosion, and surface crack growth.

Since the excitation frequency of a wave mode is inversely proportional to the wavelength, a wave mode with high frequency is preferred to generate small wavelength, and therefore be able to detect small-sized damage, as the wave is more sensitive to damage of the size larger than or equal to half of the wavelength. However, high frequency can result in presence of multiple wave modes due to the dispersive properties of Lamb waves. Power-spectral-density (PSD), which is the energy distribution of a wave in frequency domain, is used to achieve the balance between the frequency and dispersive properties of Lamb wave modes [17]. For a certain structure and damage type, the maximum PSD value of a series of Lamb wave signals among a range of potential frequencies determines the most suitable frequency because it indicates the maximum response amplitude [4]. A higher PSD value results from higher response amplitude dedicated to the excitation frequency in the diagnostic signals. As for the amplitude of the excitation frequency, the higher the amplitude of the excitation signals, the stronger responses can be generated in the diagnostic signals. Higher amplitude of the signal can increase the signal-to-noise ratio (SNR), leading to less contaminated signals. However, excessive voltage can depolarise or even damage the PZT elements. The maximum excitation voltage is generally dominated by the limitation of PZT elements given by the manufacturer.

2.2. Signal processing and feature extraction

Captured Lamb wave signal carries comprehensive information regarding to any interferences existing in the wave path. Signal processing techniques are required and able to extract the useful information from the raw signals. Hence, signal processing of the captured signal is one of crucial components of

structural health monitoring system as it determines the accuracy of Lamb-wave based damage identification. However, the process is complex due to the existence of multiple wave modes, dispersion, mode conversion, broadband noise, superposition of scattered signal and other features [3]. To overcome these challenging problems, various signal processing techniques have been developed, in particular time domain analysis, frequency domain analysis and jointed time-frequency domain analysis. In most studies, the captured wave signals are presented in time domain where the propagation of Lamb waves through structures in term of time is recorded, hence it can provide the most straightforward information about the waves. The features of Lamb waves can be extracted in time domain including the absolute value of amplitude, root mean square (RMS), Time-of-flight (ToF), etc.[4] Among these features, the ToF, i.e. the time required for a specific wave mode to travel a certain distance, is the most straightforward and important feature of Lamb waves because it indicates the relative distance between sensor and damage, therefor ToF is widely adopted by researchers to locate damage[7, 9, 18-21] and then to quantify the damage size[19].

To avoid the potential loss of information carried by Lamb waves in the sole time- or frequency- domain analysis, a combination of time and frequency domains, known as jointed time-frequency domain analysis, is also introduced. Techniques such as short-time Fourier transform (STFT) [7, 19, 22], Wigner - Ville distribution (WVD) [20] and wavelet transform (WT) [5, 23, 24] are widely applied to extract features concerning time- and frequency- information simultaneously. Beside the abovementioned conventional signal processing methods, Sohn et al [25] combined linear response subtraction (LRS) and

synchronous demodulation (SD) to extract the crack-induced spectral sidebands. Lu et al [26] proposed a signal processing algorithm using cross-correlation function to extract the arrival time of first wave component induced by damage. Yan et al [27, 28] extended STFT and developed a new signal processing method called frequency slice wavelet transform (FSWT). By comparing with conventional methods e.g. fast Fourier transform (FFT), continuous wavelet transform (CWT), discrete wavelet transform (DWT), STFT and WVD, FSWT was found to be more flexible to fit ever-changing signals and more convenient to analyse and control in application.

2.3. Data Fusion

Lamb wave-based damage identification is a typical inverse problem, in which the outcome, i.e. damage-induced wave signals, is known and then interpreted to identify the reason leading to the outcome, i.e. defects. Inverse algorithms for damage detection have been extensively examined in recent years, among which feature-based inference techniques are widely adopted for Lamb wave-based damage identification [3]. Data fusion, the process of aggregating and interpreting features extracted from captured signals, is applied to relate the extracted features to damage parameters. Damage index (DI) [29-31], time-of-flight based damage triangulation [18, 24, 32], time reversal [33, 34], migration technique [35] and probability-based diagnostic imaging [7, 36-43] are common data fusion algorithms adopted to identify the damage.

Damage index, developed from features extracted from captured Lamb waves, can be used to establish the relationship between features and damage parameters. Cho and Lissenden [29] detected fatigue crack in the vicinity of a fastener holes and inside a lap joint using transmission coefficient [44] and

transmission coefficient ratio (TCR). Lu et al [30] successfully correlated the length of a through-thickness crack with reflection coefficient (RC) and transmission coefficient [44] with the assistance of a Hilbert transform. However, DI-based damage identification, correlating a particular DI with a particular damage parameter, generally cannot define different or multiple damage parameters and the accuracy of this algorithm is strongly depending on the extracted feature. The selected DI must be most sensitive to the damage parameter of interest to avoid ambiguous identification results. To overcome this deficiency, He et al [45] proposed a multi-feature integration method based on a second-order multivariate regression analysis to detect fatigue crack and to estimate crack length in riveted lap joint.

The difference in ToFs between damage-induced and incident waves is one of the most straightforward features. Damage can be triangulated based on the difference in ToFs, and hereby the relative position among actuator, sensor and damage can be established in an ellipse shape. The intersections of the ellipse established from multiple actuator-sensor pairs can be used to indicate the possible location of the damage. Sun et al [18] applied one-dimensional ToF based triangulation to locate the notch in a thick steel beam. Hu et al [32] successfully located circular and elliptical through-thickness holes in an aluminium plate using damage triangulation with the assistance of a sensor network. Moll et al [24] extended the ellipse method to detect multiple damage in the aluminium plate.

There has been increasing interest in employing probabilistic-based diagnostic imaging (PDI) techniques for Lamb wave based SHM by visualising damage in a two- dimensional imaging. The value of the probability image at a

specific pixel, termed field value, can be applied to calculate the probability of the presence of damage at point[3, 41]. Imaging approaches can be grouped into four categories in term of DI extracted from captured Lamb waves, which are ToF [7, 42], signal amplitude, signal energy and signal correlation[38, 39]. Wu et al [38] applied a signal correlation based diagnostic imaging technique to detect debonding in a composite plate using the ratio of the energy of scattered signal to the baseline energy. Su et al [42] developed a ToF based diagnostic imaging approach to probabilistically. Zhou et al [37] applied a two-level synthetic approach combining ToF and signal intensity to indicate the orientation of individual damage edges, and later proposed a probability-based diagnostic imaging using hybrid features consisting of ToF, signal energy intensity and signal correlation [36]. The proposed PDI approach was capable of visualizing structural damage quantitatively, regardless of shape and number.

2.4. Nonlinear Lamb waves evaluation

Investigation of using nonlinear characteristics of Lamb waves to detect microscopic material degradation and defects has been of growing interest. Nonlinear evaluation methods are more sensitive to microscopic defects and capable of identifying incipient damage in contrast to linear methods. Second-harmonic generations have been employed to characterize the microscopic defects in metallic structures by many researchers [40, 46-55].When the incident Lamb waves traverse an elastic medium, the waveform of the incident waves is distorted by the inherent nonlinearities from the medium and additional nonlinearities from damages which lead to the higher-order harmonics generation [40, 47, 48, 51] in the acquired Lamb waves. Higher-order harmonic

generation is the most classical nonlinear acoustic phenomenon, only up to second-order harmonic is considered by researchers [40, 49-58] because the nonlinearity of third- or higher orders is much smaller and therefore difficult to detect. In general, cumulative second-harmonic generation of Lamb wave propagation does not occur, only if several conditions are satisfied. Deng [48] reported the physical process of cumulative resonant second-harmonic generation of Lamb-mode propagation in an isotropic solid plate. The results indicated that the cumulative second-harmonic field was symmetrical regardless of whether the Lamb wave mode propagated symmetrically or anti-symmetrically. Phase velocity matching between the primary waves and second-harmonic was required. Lima and Hamilton [59] investigated harmonic generation in elastic isotropic plates where all mods of secondary wave field were considered. It was found that the amplitude of the secondary Lamb wave mode grows linearly in the direction of propagation if phase matching and non-zero power flux from primary to secondary wave are satisfied. Lee et al. [58] proposed two additional conditions for cumulative harmonic generation, which were group velocity matching and non-zero out-of-plane displacement. The phase and group velocity matching is named synchronism. This warrants a smooth power transfer from primary mode to the generated secondary mode of the same mode type, and the primary and secondary wave arrive at the same time on the same received point.

When an ultrasonic wave with high amplitude is incident on imperfect surfaces, repetition of collisions between the contact surfaces occurs, and therefore higher harmonic responses are generated. This effects is known as contact acoustic nonlinearity (CAN) [60]. When ultrasonic waves reach the

imperfect contact surfaces, “breathing” behaviour of the interface occurs under cyclic loading. The compressional part of the waves can close the interface and allow the compressional part to penetrate, while tensile part opens the interface and therefore cannot be transmitted through the interface[52, 57], as illustrated in Figure 2-1. The penetrated waves result in a localised nonlinearity, CAN, which can be detected by higher harmonics. This imposes an additional nonlinearity to the ultrasonic wave signals guided by medium [52]. CAN has attracted increasing attention and has been applied to characterise closed defects and imperfect interfaces [52, 60-65].

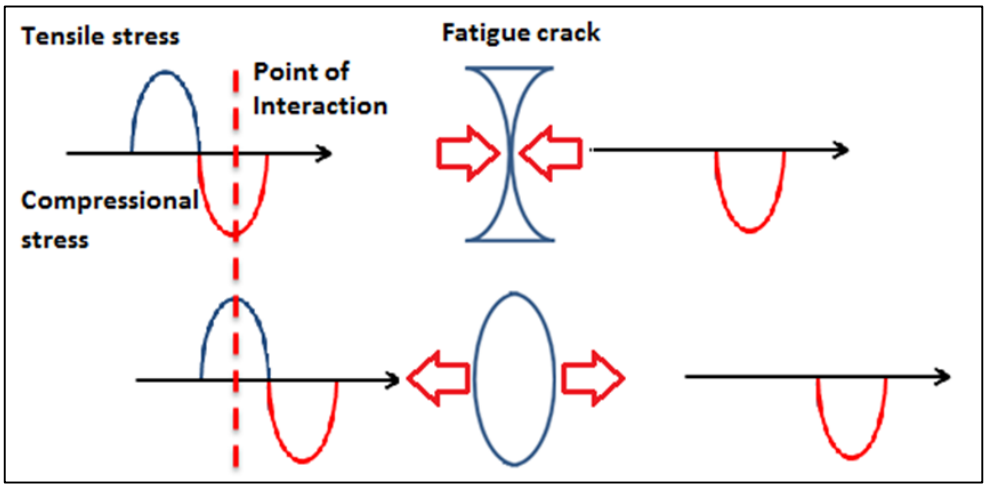

Figure 2-1 Schematic diagram illustrating CAN [52, 57]

A recent paper [56] provided a comprehensive review on the latest advances in nonlinear guided wave based non-destructive evaluation, covering theoretical modellings, numerical simulations and experimental validations.

Pruell et al. [50] developed an experimental procedure for nonlinear Lamb wave based detection of fatigue damage in metallic plates. The results showed the normalised nonlinearity of Lamb waves was related to fatigue damage which was similar to that of longitudinal and Rayleigh waves. The relationship

between acoustic nonlinearity and fatigue damage was further confirmed with the measured cumulative plastic strain.

Dutta et al. [54] conducted an experimental study to detect fatigue crack in aluminium and steel structures using nonlinear Lamb waves. Noticeable harmonics in response signals from cracked specimen were observed. Less effect of nonlinearity was observed in the case of steel structure. This was because the size and stiffness of the steel specimens were much greater than those of aluminium plates, the amplitude of vibration in steel was smaller for the same level of excitation voltage. The presence of second- and third harmonics in the undamaged and notched states caused by unknown sources was also reported.

Hong et al. [52] developed a modelling technique for comprehending nonlinear characteristics of Lamb waves travelling in a fatigued medium. Material, geometric, plasticity-driven, and CAN were considered in this model. An experimental study was later conducted to verify the reliability of the proposed modelling technique and a good consistency was obtained between the results from the simulation and experiments.

2.5. Research gap and research aim

Lamb wave-based SHM in plates has attracted extensive research interest during the past decades. In particular, Lamb wave-based detection of fatigue cracking in thin metallic plate-like structures have been studied by [20, 29, 32, 35, 66]. However, limited studies have been done in the area of monitoring crack growth and detecting fatigue crack initiation in composite retrofitted metallic systems in civil engineering because of the complexity of wave

propagation in anisotropic infrastructures, where cracking is concealed. There has arisen an increasing interest among researchers to study the ability of using nonlinear Lamb waves to detect different types of damages due to its sensitivity to detect small-scale defects. However, current studies only focus on detecting defects in thin homogenous metallic plates, such as aluminium plates, no study, to the best of author's knowledge, has been carried out to determine the feasibility of using nonlinear Lamb waves to detect concealed small-scale damage in multiple layered sandwich structure consisting of different materials. From the point of view of civil infrastructure evaluation and monitoring, the most commonly used evaluation techniques are visual inspection, dye penetrant inspection and passive ultrasonic testing, which are labour intensive and these techniques require up-close access to the structure for fully-developed crack detection. Employing Lamb wave-based SHM technique in civil infrastructure evaluation can provide more timely and accurate information about the structural health than conventional methods with less cost and labour requirements. Hence this method is introduced into this study to monitor the structural health of both steel plates and CFRP strengthened steel plates.

The specimen used in this study is a multi-layer plate-like structure consists of 3 materials, i.e. steel, epoxy adhesive and FRP. Since Lamb waves are sensitive to material changes, the wave velocity varies along different materials, complicating the interpretation of the signals. Furthermore, beach marking technique is widely adopted by researchers [67, 68] to estimate the fatigue cracking propagation in FRP strengthened steel plates, which however can only be visualised after the specimen failure, limiting the applicability in practical application. To overcome the complexity of Lamb waves propagating in multi-

layered structure and the deficiencies of the currently used techniques, a new non-destructive, real-world applicable methodology will be designed in this study to monitor the propagation of cracking in FRP strengthened steel plates subjected to fatigue loading. The key aims of this project are:

- To assess the feasibility of using linear Lamb wave-based structural health monitoring technique to monitor concealed fatigue crack propagation in CFRP strengthened steel plates.
- To assess the feasibility of using nonlinear Lamb wave-based structural health monitoring technique to detect concealed fatigue crack initiation in CFRP strengthened steel plates.

In order to achieve these aims, the key objectives are proposed and listed as follow:

- To investigate the propagation of linear and nonlinear Lamb waves in multi-layered structures consisting of different materials. This is studied in order to understand the dispersive characteristics of Lamb waves when travelling in multiple-layered specimens. The findings are used to help design sensor network and select excitation wave modes.
- To study the interaction of Lamb wave modes with fatigue cracking, to detect crack location and to monitor the crack propagation. This is studied in order to assess the sensitivity of the proposed method to detect cracks. The objective is first assessed using finite element method, then is assessed through experiments.

- To monitor the crack propagation and to evaluate the initiation of fatigue cracking. This part is devoted to assess the feasibility of using proposed methods to detect defects and its sensitivity to defects.
- To assess the methodology under different loading condition. This is studied in order to assess the feasibility of using proposed methods to detect defects and its sensitivity to defects under different loading conditions.

2.6. Summary

The literature review briefly summarised a great number of studies relate to development and researches of applying Lamb waves on damage detection, including debonding, delamination and fatigue cracks. The key components to generate Lamb waves were discussed, which were the transducer, wave mode, wave frequency, and waveform. The S0 and A0 modes were compared and discussed. The commonly used signal processing techniques and damage recognition methods were presented. The physical mechanism and nature of nonlinear Lamb waves were presented in detail in this chapter, alongside with the latest numerical and experimental studies on applying nonlinear Lamb waves to detect fatigue cracks.

Chapter 3. Methodology

The methodology for Lamb wave-based SHM was presented in this chapter. Firstly, the specimen configuration and the material properties were summarised, followed by the selection of wave mode, waveform and the excitation frequency, and the damage detection strategy. Secondly, the numerical method was described covering the mesh convergence study, modelling strategy for signal excitation and acquisition, and modelling of damages. Lastly, the experimental method was discussed, including the specimen preparation and test set-up.

3.1. Specimen

3.1.1. Specimen configuration

The configuration of the specimens used in this project was designed to be similar to those in [67] for comparison and correlation purposes. The specimens were made of a steel plate with a through-thickness hole at the centre and two CFRP laminates bonded to the upper and lower surfaces of the plate by epoxy adhesive. The detailed geometry and configuration of the specimens are presented in Figure 3-1. The steel plate was 500 mm long, 90mm wide and 10 mm thick. A through-thickness hole of 2.5 mm radius with an initial notch of 1 mm long and 0.3 mm wide was drilled at the centre of the plate to facilitate the propagation of cracking. Two 250 mm long, 90 mm wide CFRP laminates were bonded to both upper and lower sides of the specimen. Six surface-mounted circular PZT sensors, with 10 mm in diameter, were placed on the upper side of the specimen as shown in Figure 3-1 (c).

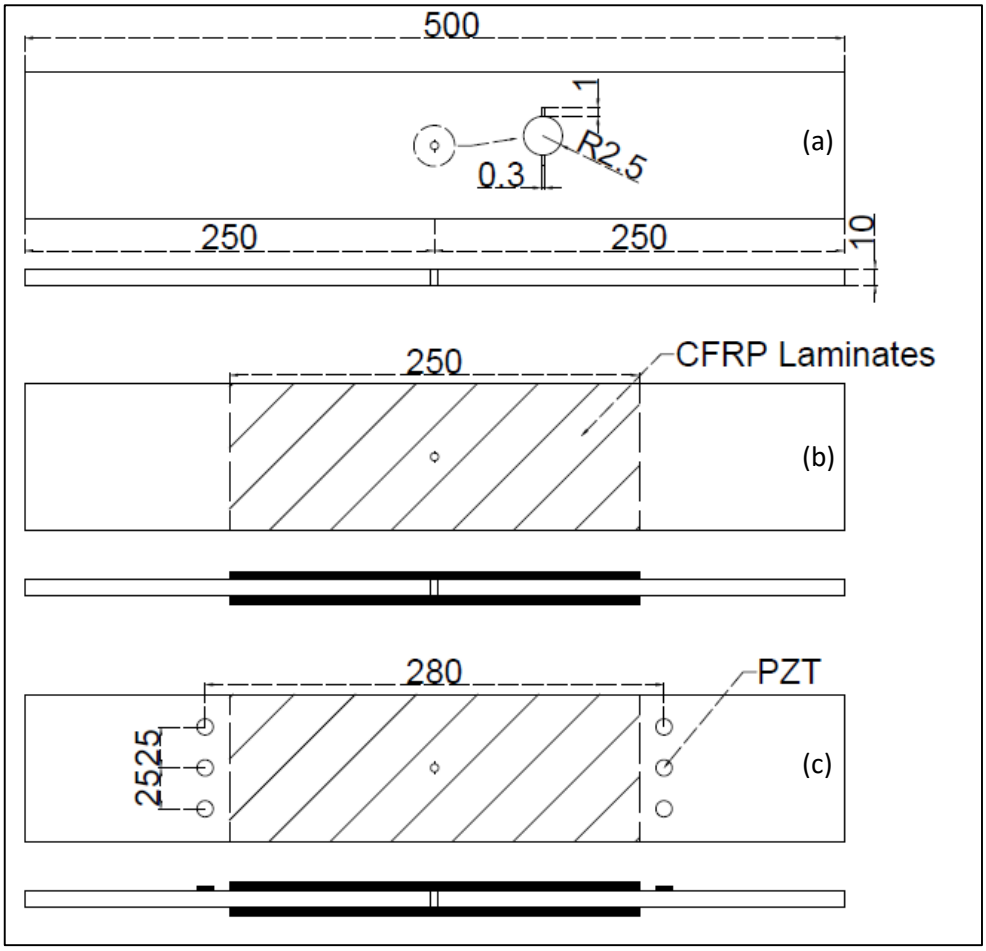

Figure 3-1 Specimen geometry (in mm) and configuration (a) Steel plate with through-thickness hole and crack (b) CFRP strengthened steel plate (c) Layout of PZT sensors

3.1.2. Material properties

The steel plates are Grade 300 Hot rolled plates with the nominal tensile strength of 450-540 MPa and the density of 7850 kg/m^3. "MBrace^{TM} Laminate 210/3300" manufactured by BASF were adopted to strengthen the steel plates. It is an ultra-light weight high modulus plate with typical nominal strength of 3300 MPa and a nominal tensile modulus of 210 GPa. The measured thickness is 1.47 mm with the same width of 90 mm as the steel plate. Araldite 420 A/B epoxy adhesive was used to bond CFRP laminates to the steel plate. The

material properties of steel plates and CFRP laminates were tested according to ASTMD3039 in Civil Laboratory, Monash University by [67]. The measured material properties of steel and CFRP plates are listed in Table 3-1.

Table 3-1 Measured material properties of steel and CFRP plates

	Steel	MBRACE^{TM} Laminate 210/3300	Araldite 420 A/B
Density (kg/m^3)	7850	1900	
Tensile strength [MPa]	497	2882	28.6
Tensile modulus (GPa)	200	177	1.901
Thickness (mm)	10	1.57	

3.2. Selection of wave mode, waveform and excitation frequency

Lamb waves are highly dispersive with multiple modes propagating simultaneously at different velocities across all excitation frequencies. The dispersive characteristics of Lamb waves complicate the selection of wave modes and their measurement, which limited the implementation of ToF methodologies. Two important parameters of the dispersive characteristic are phase and group velocities, which are dominated by the properties of the medium, the thickness of the medium and the frequency. A commercial software known as "DISPERSE®"[69] has been adopted in this study to calculate dispersion curves, which are displayed in Figure 3-2 for a normalised thickness steel plate These curves demonstrate, phase and group velocities of Lamb wave modes plotted against frequency-thickness production.

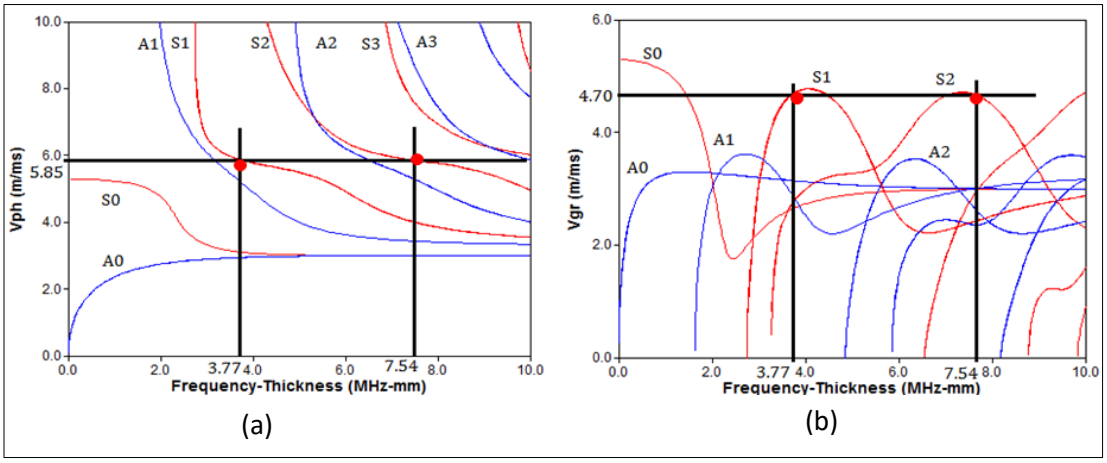

Figure 3-2 a) Phase and b) group velocity for a 10mm thick steel plate calculated using DISPERSE®

In this study, both linear and nonlinear Lamb waves will be employed. The central excitation frequency of linear Lamb waves is selected below the cut-off frequency where higher-order Lamb waves start to present, so as to minimise signal complications due to the presence of higher-order harmonics. For nonlinear Lamb waves, fundamental modes are excited at selected frequencies, which simultaneously satisfy the conditions of synchronism and non-zero power flux as discussed in Section 2.4. As illustrated in Figure 3-2, Mode pair (S1, S2) satisfies both synchronism and non-zero power flux. The excitation frequency of S1 mode is at 3.77 MHz·mm, which can induce a S2 mode at 7.54 MHz·mm. Both S1 and S2 mode propagate at the same phase and group velocities. As illustrated in Figure 3-3, two waveforms have been used in this study. A 5.5-cycle tone burst is used to excite the linear Lamb waves, in consideration of minimizing the possibility of wave packet overlapping and narrowing bandwidth so as to minimise wave dispersion. To enhance the recognition of second harmonic mode, the cycle number of the tone burst is increased to 15.5, which reduces the wave bandwidth. The signal energy is

more concentrated around the excitation frequency, where the peak amplitude increases and accordingly wave dispersion is minimised.

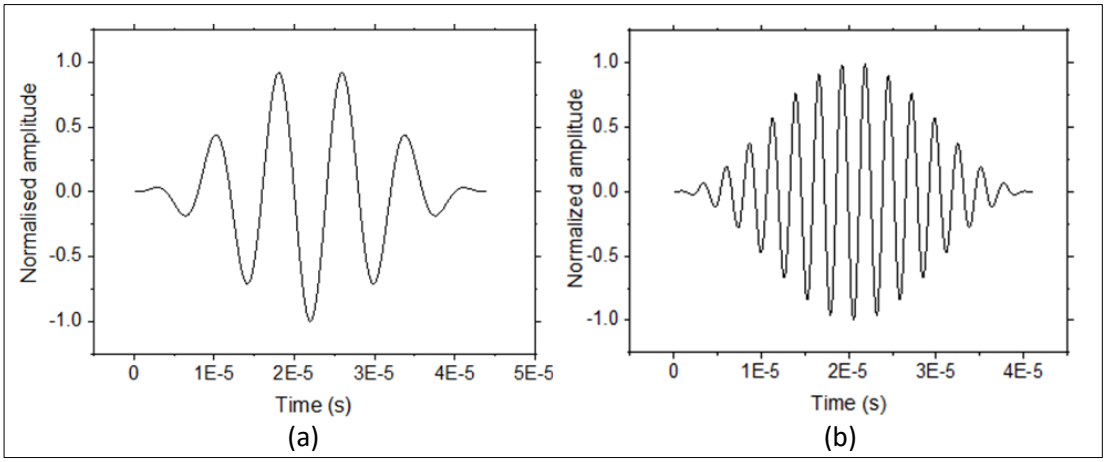

Figure 3-3 a) 5.5-cycle and b) 15.5-cycle Hanning-windowed tone burst

3.3. De-noising of signal

Operational and environmental noises are unavoidably received by PZT sensors and recorded as part of the signal. These noises contain useless information about the structure and mask the desired Lamb waves, complicating the interpretation process of the received signals and leading to a false structure health diagnosis. It is therefore important to remove the noises from the signal to generate the desired ones. A discrete wavelet transform, particularly Doubechies wavelet, is employed to de-noise the received signals, where the original signal is decomposed into different levels of signal components through a series of frequency filter as shown in Figure 3-4. The maximum frequency of the original signal for decomposing is half of the sampling rate of the received signal. At each decomposition level, the signal is halved into lower and higher frequency range and then the signal in lower frequency range is further halved until it contains the frequency of activated Lamb wave mode.

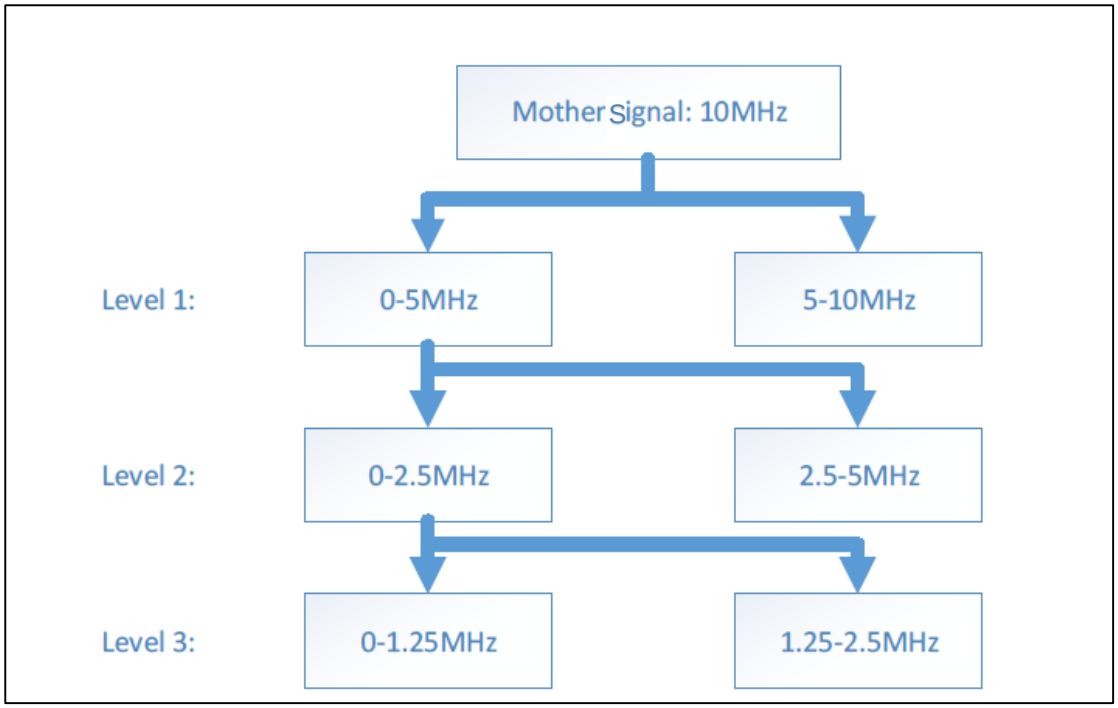

Figure 3-4 Principle of DWT-based signal decomposition

3.4. Damage detection strategy

As discussed in literature review, time-of-flight (ToF) is the most straightforward feature that is related to the interference of developed cracks within the structure, hence it is suitable as a damage index (DI) to detect the crack propagation. The ToF of damage-scattered waves (linear method) and damage-induced waves (nonlinear method) can be applied to extract the length of the wave propagating path, therefore the damage can be triangulated to determine the relative positions of the actuator, sensor and damage. Furthermore the crack propagation can be monitored by detecting the wave path increment due to the crack growth. To calculate the length of the wave path, the wave velocity travelling in the specimen must be identified primarily. The velocity of all wave paths which are not influenced by the initial notch, e.g. paths S2-S4, S3-S6, S2-S5 as shown in Figure 3-5, is calculated. The average value of these velocities is chosen as the benchmark wave velocity travelling in

the specimen. The relative distances between damage *(x, y)* and the actuator and the sensor, $D_{a,i}$ and $D_{i,s}$,are presented in an ellipse shape, as illustrated in Figure 3-6. The intersection of the ellipses derived from different pitch-catch transducer pairs is used to identify the possible location of the crack, as shown in Figure 3-7.

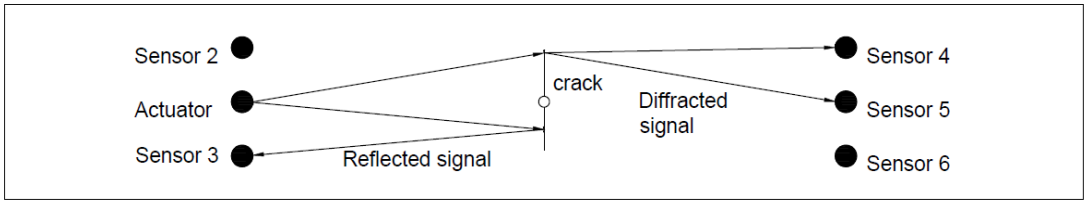

Figure 3-5 Wave paths for reflected signal and diffracted signal

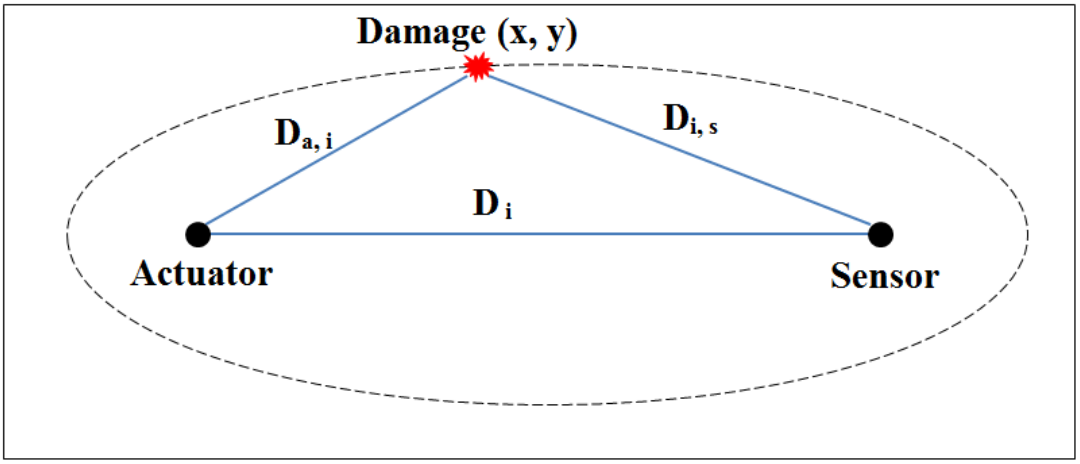

Figure 3-6 The illustration of relative distance

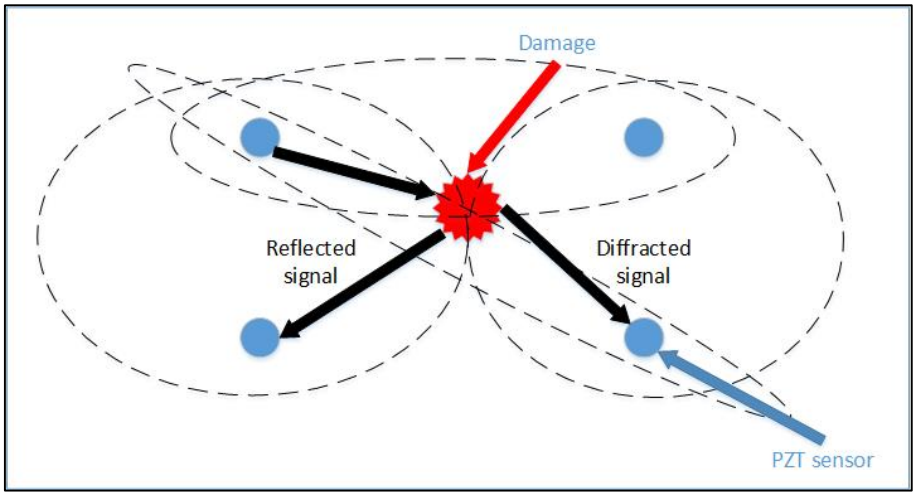

Figure 3-7 Principle of damage triangulation

Probability based diagnostic imaging (PDI) approach is employed to better visualise the damage and detect the probability of the presence of the damage at a specific location. Assuming that there are N sensing paths in a sensor network, the probability of damage present at specific location (x, y) can be calculated as [70]

$$P(x,y) = \sum_{i=1}^{N} DI_I \cdot W_i[R_i(x,y)] \qquad [3.1]$$

Where, DI_i is the damage index for *i*th sensing path. $W_i[R_i(x, y)]$is the weight distribution function of the *i*th sensing path. It depends on the relative distance from the defect to the *i*th sensing path and can be calculated as

$$R_i(x,y) = \frac{D_{a,i}(x,y)+D_{i,s}(x,y)}{D_i} - 1 \qquad [3.2]$$

Here, D_i is the distance between the actuator and sensor for *i*th path. $D_{a,i}$ (x,y) and $D_{i,s}$ (x,y) are the distances between defect (x, y) and the actuator and sensor for *i*th sensing path, respectively.

This weight is the non-negative linearly decreasing weight distribution function of the ith sensing path when the relative distance increases [70], since a defect would cause less signal change in the incident wave path if the defect is away from the wave path [70]. The weight distribution function, which regulates the affected area of the a damage on a sensing path, can be written as

$$W_i[R_i(x,y) = \begin{cases} W_0 + Ae^{-\frac{[R_i(x,y)-R_c]^2}{2w^2}} & ,R_i(x,y)<\beta \\ 0, & ,R_i(x,y)\geq\beta \end{cases} \quad [3.3]$$

Where, W_0 is the offset (W_0=1), A is the height of the peak, R_c is the central position of the peak (R_c = β) and w controls the width (w=0.2902×β) [70]. β is the scaling parameter that controls the size of the affected elliptical distribution zones of each sensing path. Each sensing path contributes a probabilistic image of damage, where the higher field value indicates a higher chance of presence of damage in that point. To neutralise the effect of the scaling parameter on the identification accuracy, the probabilistic images constructed using all sensing paths are fused [70].

3.5. Numerical method

Numerical studies have been used alongside laboratory work as complementary and cost-effective methods to study Lamb wave behaviours and to predict the experiment outcomes. A number of numerical methods can be used to analyse Lamb wave propagation, including finite difference equations, finite element (FE) analysis, boundary element method (BEM), finite strip elements (FSE), mass-spring lattice model (MSLM) and local interaction simulation approach (LISA) [71]. Although all the approaches can provide reasonably accurate analysis of Lamb wave behaviour, FEM is the most

commonly used technique because it is the most cost-effective method. FEM can model complex geometries and determine the response at any points of a structure. A commercial FEM software Abaqus Dynamic/Explicit® has been widely used for the analysis of engineering problems, including simulation of Lamb wave propagation. Therefore, it was adopted to simulate the experimental specimens in this study.

3.5.1. Mesh convergence

Since the through-thickness hole, thin notches and circular PZTs are introduced in this model, an isotropic square mesh throughout the model cannot be achieved. A mesh convergence study was conducted, aiming for generating an appropriate mesh for the FE modelling with minimum computational costs and accurate calculation. Due to the restrictions of FEM on the degree of freedom (DOF), at least eight elements per wavelength and a minimum of four to five nodes in the thickness direction are required to achieve accurate solutions [3, 4]. To avoid calculation errors, the size of nearby elements should be similar, and for each individual element, the size in any one dimension should not be excessively larger or smaller than any other dimensions. [72].

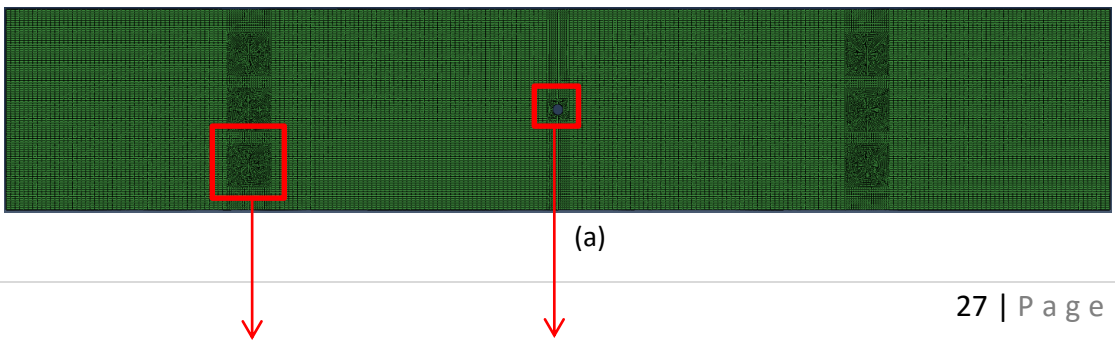

(a)

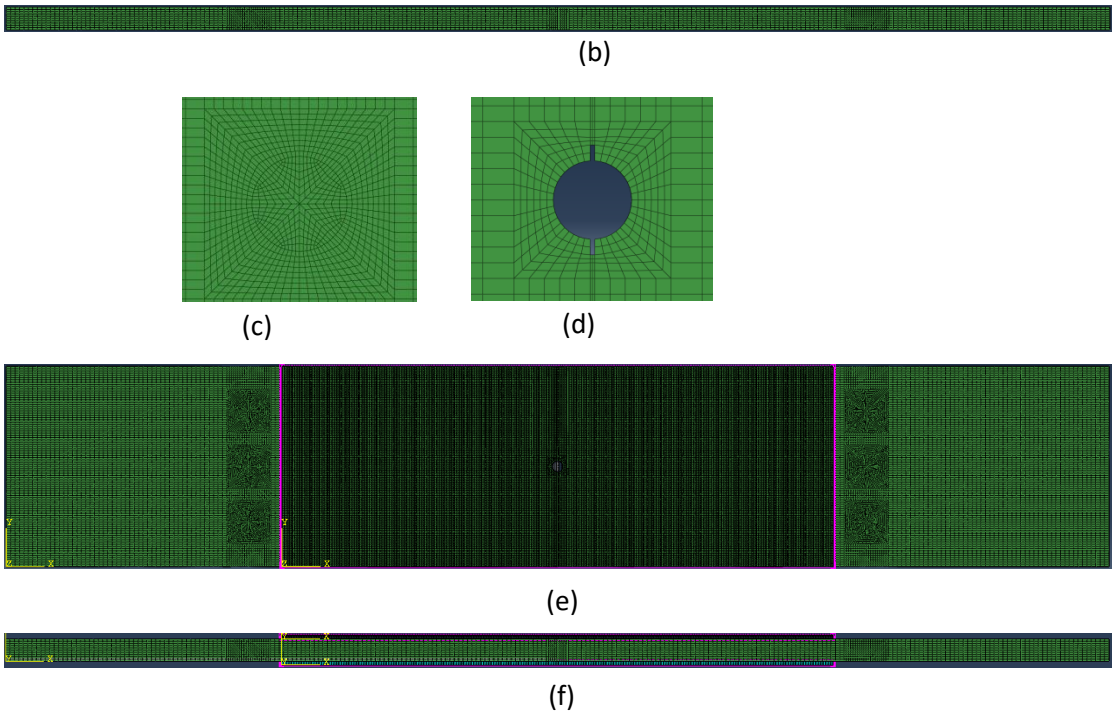

Figure 3-8 Finite element model in Abaqus a) Top view of steel plate b) Side view of steel plate c) modelling of a PZT d) modelling of damage e) Top view of CFRP strengthened steel plate and f) Side view of CFRP strengthened steel plate

The model is meshed using eight-node brick elements (C3D8R). Each node has 3 degree of freedom (x-, y- and z- axis). The model consists of four parts, i.e. the steel plate, the CFRP laminates, the adhesive layer and the PZTs. Three seed sizes are used to generate the convergence results. A seed size of 1 mm is used for the PZTs, the hole and the vicinity regions. A finer seed size of 0.5 mm is used for CFRP layers and the regions along the crack propagation direction. The seed size of the rest parts is 2 mm. The seed sizes along the thickness direction are 0.5 mm and 1 mm for CFRP laminate and steel plate respectively. The total number of elements is 287,560 and 827,560 for bare steel plate and CFRP-strengthened steel plate respectively, as shown in Figure 3-8, which can suffice for producing convergence results.

3.5.2. Signal actuation and acquisition

The transducers used in this study were Lead zirconate titanate (PZT) disc manufactured by PI®. The PZT has been modelled as a disc partitioned out of the steel plate model with the same diameter as the one used in experiments. Since the strain is transferred from PZT to the host structure through the bond layer, the response of the excited signal is activated at the contact surface of the PZT and host structure. As circular PZT could activate Lamb waves with equal magnitude omnidirectionally, the time varying forces at a maximum amplitude of 0.1 N were excited by applying uniform in-plane concentrated loads on the nodes along the periphery of the actuator to simulate the Lamb wave excitation from the circular PZT as shown in Figure 3-9. The Lamb waves therefore propagate omnidirectionally from the actuator as shown in Figure 3-10.

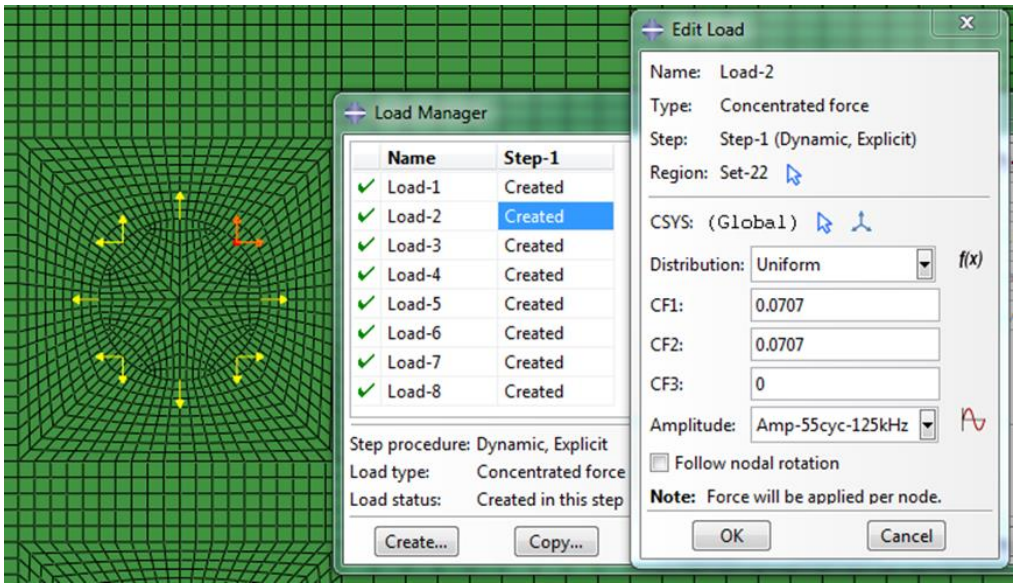

Figure 3-9 PZT model and forces

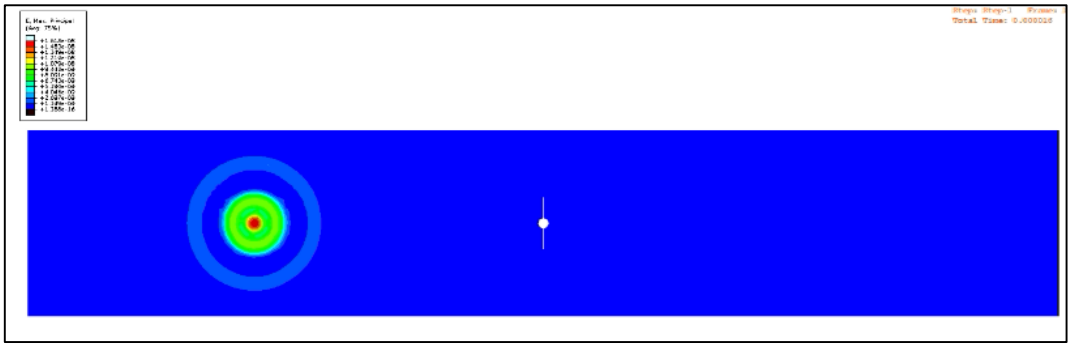

Figure 3-10 Simulation of Lamb waves propagating from the PZT model

3.5.3. Modelling of damage

Three crack modes have been simulated to study the Lamb wave behaviour under different damage conditions, including the loaded fatigue crack propagation, loaded and unloaded fatigue crack initiation.

For the loaded fatigue crack propagation, it was assumed that the specimen was under loading throughout the fatigue progress. Therefore, the fatigue crack was simulated as an open crack. The elements along the crack propagation direction were sequentially removed to simulate the crack growth.

Nodes of the elements were duplicated along the damage while keeping both surfaces in contact to create a closing crack. An Abaqus built-in function “seam” was imposed to each surface of the cracks to simulate the initiated fatigue crack[52], as shown in Figure 3-11. A surface-to-surface contact with small sliding and associated properties were imposed on the crack interfaces. This enabled the “breathing” behaviour when waves transverse the crack and therefore produced CAN.

To model the initiated fatigue crack under loading, a model was first analysed using Static/General procedure to generate the deformed model due to the static load. Then the deformed model was imported into a new model as a Part

for the wave propagation study. The CAN was simulated using the same method as described above.

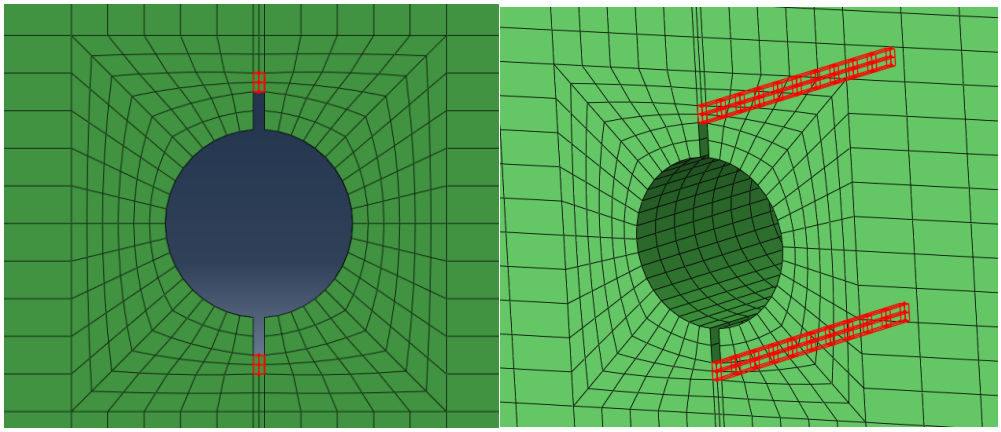

Figure 3-11 "seam" cracks to enable CAN

3.6. Experimental methods

3.6.1. Specimen preparation

The specimens were prepared in Civil Laboratory, Monash University. The bond regions of the steel plates were sandblasted to roughen the surface for adhesive bonding. Acetone was used to remove contaminates from the sandblasted areas. CFRP laminates were cut into designed configuration by technicians in Civil Laboratory. Then the CFRP laminates were bonded to one side of the steel plate by mixing Araldite 420 A/B epoxy adhesive of 10:4 w/w ratio. The specimens were cured for 24 hours before bonding CFRP to the other surface of the steel plate. A concrete block was placed on top of each specimen to squeeze out the excessive adhesive and air bubbles to achieve uniform thickness of adhesive layer, and to prevent formation of initial debonding. The specimens were cured for at least 2 weeks at room temperature to achieve full strength of adhesive layers. Six circular PZT sensors was then bonded to each specimen by UHU® SUPER all-purpose adhesive according to the designed

layout as shown in Figure 3-1 (c). A weight was placed on each PZT sensor during curing to create a thin, stiff and uniform bond layer, as the bond layer strongly affects the strain transfer from PZT to the host structure. Twin-core cable was wired to the positive and negative pole of PZT by soldering iron. The completed specimen was shown in Figure 3-12.

Figure 3-12 Steel plate and CFRP strengthened steel plate with surface-mounted PZT sensors

3.6.2. Test set-up

The fatigue tests were performed using Instron 8802 servo hydraulic testing machine located in Civil Laboratory, Monash University. Sinusoidal cyclic tensile loads were applied, with a frequency of 30 Hz, and a stress ratio (minimum load/maximum load) of 0.1 [67]. The maximum stress was set to be 150 MPa, which is about 30% of ultimate strength of the steel and 46% of the yield strength, which resulted in a maximum load of 135 kN and a minimum load of 13.5 kN. The beach marking technique was employed to indicate the crack propagation by inserting a lower stress range and a shorter number of cycles to the original fatigue cycles [67]. The maximum stress was kept

constant but the stress ratio was increased from 0.1 to 0.55. Therefore, beach marks were left on the cross-section of the specimen due to the changes in stress intensity factor at the crack tip and crack propagation rate. Moreover, a lower frequency of 10 Hz was assigned for the beach marking cycles to ensure a smooth transformation between normal and low stress range cycles. The test procedure was summarised in the flow chart as shown in Figure 3-13.

A sinusoidal tone burst was inputted into a Tektronix AFG3102 arbitrary function generator. The amplitude of the signal was then amplified by 100 times using a Ciprian electronic high-voltage power amplifier. The signal was then applied to one PZT disc as an actuator and sent through the specimen. Signals received by sensors were acquired by a Tektronix DPO4043B digital phosphor oscilloscope and transformed into digital data. The data were then saved to

external hard drive in csv file for signal processing. The procedure of data acquisition is shown as in Figure 3-14.

A sensor network was employed by using different PZT sensors as actuator sequentially. The overall set-up with the fatigue test machine and SHM instruments are illustrated in Figure 3-15.

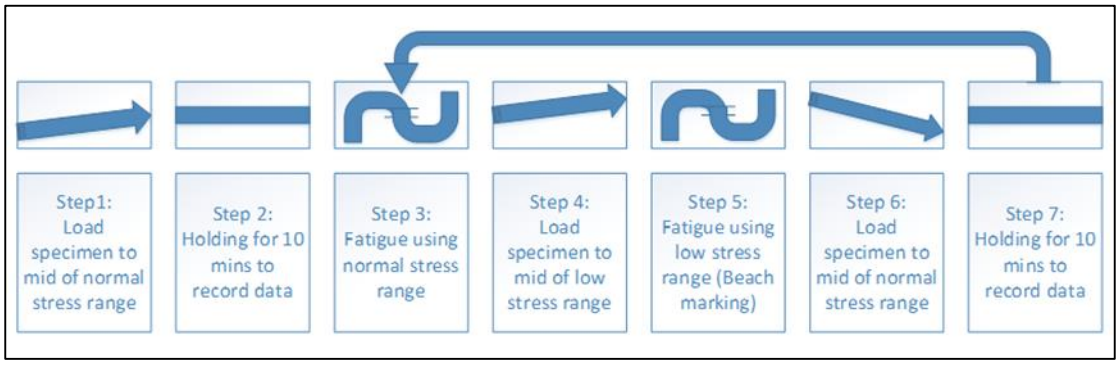

Figure 3-13 Fatigue test procedure

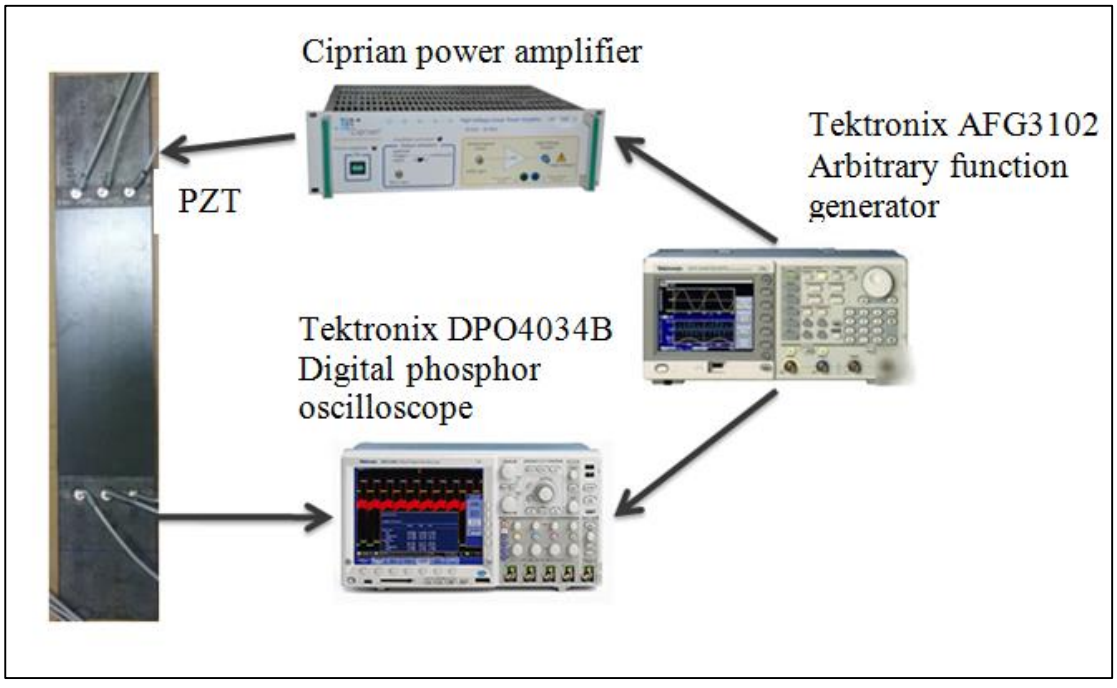

Figure 3-14 Data acquisition procedure

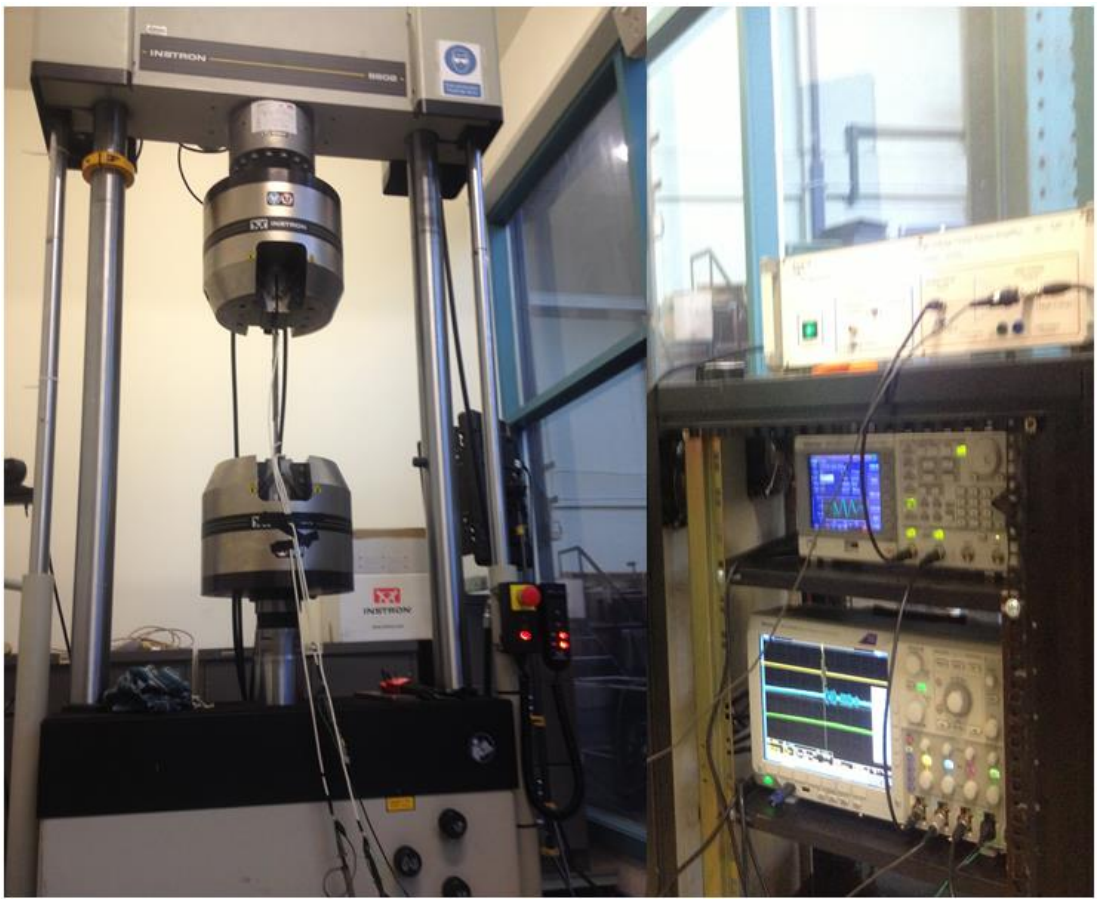

Figure 3-15 Test set-up

3.7. Summary

The methodology developed and implemented for the numerical and experimental studies was presented in Chapter 3. The configuration and material properties of the specimen were presented. The key features to design an excitation signal were discussed in term of wave mode, waveform and excitation frequency. A Doubechies wavelet was adopted to de-noise the signals. Time-of-Flight (ToF) was employed as the key feature to detect the damage. The proposed methodology based on probability diagnostic imaging (PDI) was addressed for the purpose of better visualizing the location and severity of the damage. The numerical modelling and experiment setup were introduced as well.

Chapter 4. Monitoring fatigue crack propagation using linear Lamb waves

In this chapter, Lamb waves were applied to monitor the crack propagation via numerical simulation and experimental validation. Firstly, the selection of excitation frequency was discussed. Signals at a wide range of frequencies were excited and the response amplitudes of the S0 mode were obtained to select the most suitable frequency. Then this frequency was used to excite S0 mode in the three-dimensional CFRP-strengthened steel plate model, followed by the experimental validation.

4.1. Excitation frequency

The excitation frequency of Lamb waves has significant effects on the detectability of defects, on the basis of which, frequencies, from 75 kHz to 175 kHz with an increment 25 kHz, were evaluated in this study to find the optimal frequency with the strongest signal amplitude. The peak amplitude of the signals at different frequencies were extracted and summarised in Figure 4-1. It is clear that the strongest signal occurred at a frequency of 125 kHz for the first wave package with the fastest propagation velocity, which is recognised as S0 mode. It is thereby concluded that this frequency was the most appropriate for the damage detection and would be used as the excitation frequency for FE modelling

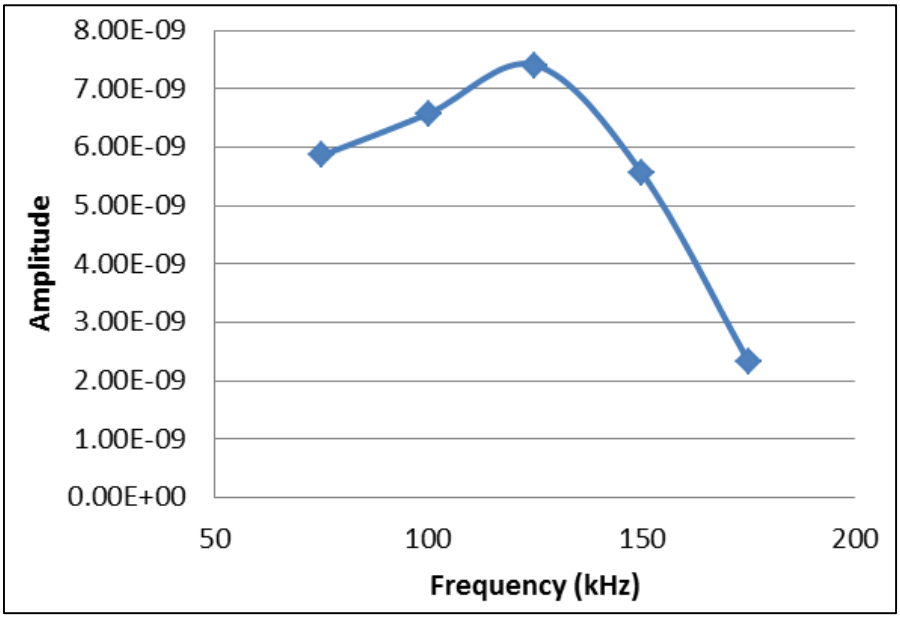

Figure 4-1 Maximum amplitude of the signals against frequencies

4.2. Model analysis

The feasibility of using linear Lamb waves to monitor fatigue crack propagation is first assessed numerically. Three-dimensional models of CFRP-strengthened steel plate models with different crack lengths were conducted. The models are based on the experimental setup, where CFRP-strengthened steel plates of 500 mm×90 mm×10 mm consists of one through-thickness hole and two notches located at the centre as illustrated in Figure 4-2. Signals captured in this model are assumed to be the benchmark state. The notches are artificially extended to a certain length to simulate the crack propagation due to the cyclic loadings, as illustrated in Figure 4-3. The growth rate of the crack is set to be 1mm per model up to 20 mm of crack extension, and then the growth rate is increased to 5mm per model up to 35 mm. the signals received in these models are assumed to correspond to different propagation status of a fatigue crack.

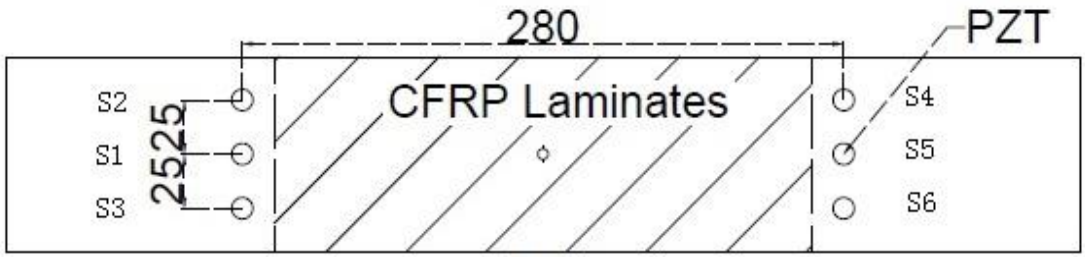

Figure 4-2 Diagram of CFRP-strengthened steel plate with surface mounted PZTs

The material properties of steel used in this model is same as those in Table 3-1. Since the CFRP is an anisotropic material, the elastic properties of CFRP model are defined as engineering constants, which are summarised in Table 4-1.

Table 4-1 Engineering constants for CFRP

E1	E2	E3	Nu12	Nu13	Nu23	G12	G13	G23
177.000	177,000	17,000	0.32	0.32	0.45	4,500	4,500	2,500

The excitation frequency of 125 kHz is selected, which enables the presence of only fundamental S0 and A0 Lamb wave modes in the steel plate. A 5.5 cycle tone burst is excited by applying time varying concentrated forces on the nodes along the periphery of the actuator and the magnitude of the force is set to be 0.1 N, which is equivalent to the maximum response of a PZT disc. The signals captured from path S1-S5 at 125 kHz are displayed in Figure 4-4. The black solid lines represent the signals in benchmark state, while the red and blue solid lines represent the crack state with crack length of 2mm and 15mm respectively. The first arrival wave package is the transmitted fundamental symmetric S0 mode, followed by the transmitted fundamental antisymmetric A0 mode. All boundary-reflected waves arrived after A0 mode. The transmitted S0 mode is selected for computing the damage index in this study. It is noted that

the S0 mode in path S1-S5 is not a clear 5.5-cycle Hanning windowed tune burst, while, a clearly defined 5.5-cycle Hanning windowed S0 mode is captured in path S2-S4, as illustrated in Figure 4-4 (b). It is because the transmitted waves are scattered when interacting with cracks, and thereby affect the wave propagation. The A0 mode arrives at the sensor before the S0 mode passes through the sensor completely, causing partial overlapping of the S0 and A0 modes. As can be seen, the ToF increases while crack length increases, implying that the presence of a crack in the sensing paths increases the length of wave propagation route. Noticeable amplitude drop, as the crack length increases, can also be observed resulting from more wave energy being reflected by the longer crack, and thereby less energy in the transmitted waves can be captured by the sensor.

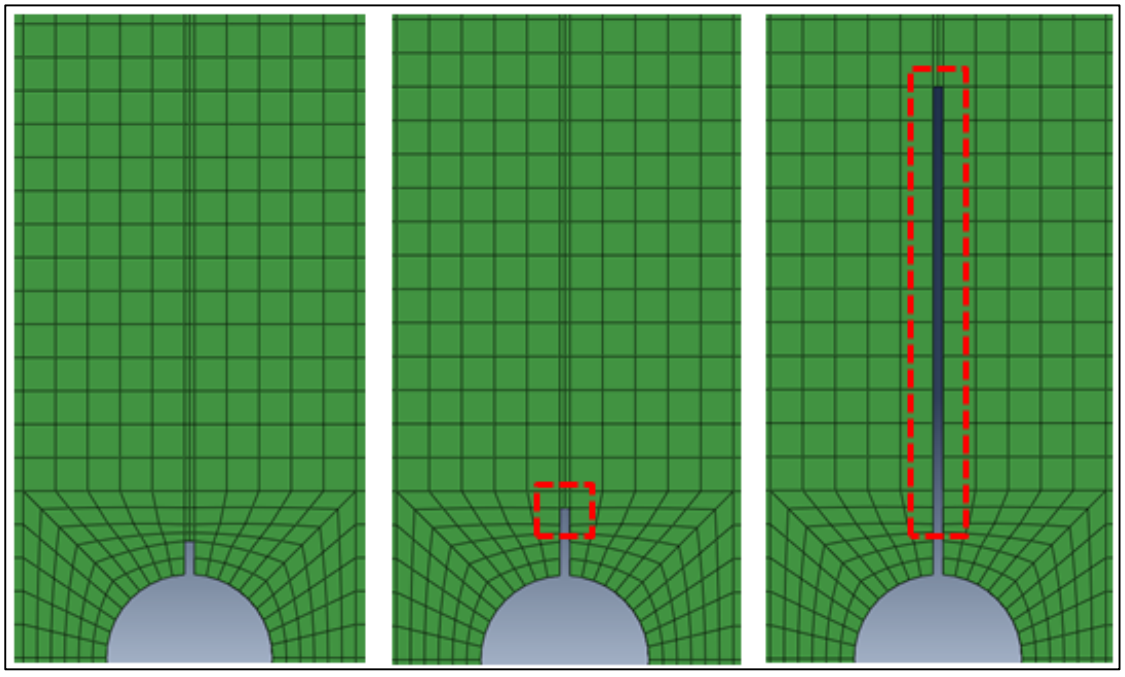

Figure 4-3 Simulation of damage a) benchmark state b) crack state (2mm), and c) crack state (15mm)

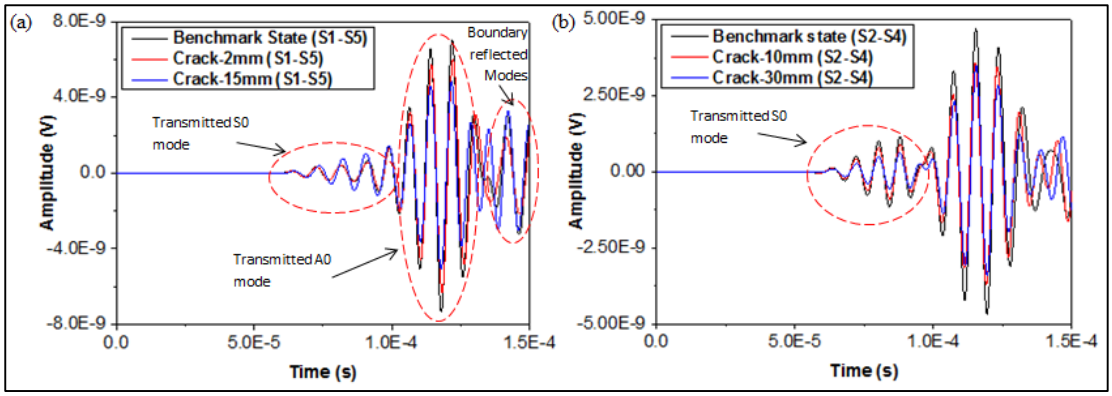

Figure 4-4 Sample waveforms captured in sensing path S1-S5 and S2-S4

The damage index, ToF, of the first arrived S0 mode was extracted from the captured signals. Due to the symmetricity of the model, 5 sensing paths, S1-S5, S1-S6, S2-S4, S2-S5, and S2-S6, were selected to monitor the crack growth, as illustrated in Figure 4-5. In sensing paths S1-S5 and S2-S6, the crack directly encountered with the sensing path from the benchmark state. It was expected that the crack affected the first arrived transmitted S0 mode from the very beginning. In sensing paths S1-S6 and S2-S5, the crack encountered with the sensing paths when the growth of crack reached 10mm. Insufficient crack length estimation was thus expected at the small crack length (< 10 mm). As sensing path S2-S4 was away from the crack, it was the least effective sensing path to detect the crack growth as the crack only encountered with the sensing path until the crack length of 22.5 mm.

The benchmark signal is defined as the captured signal in those sensing paths, where there is no defect to scatter the Lamb waves. The velocity of Lamb wave is calculated by averaging the velocity of the first 3 valleys of the S0 mode in the captured signals to minimise the dispersion effects on the signal.

4.2.1. Simulation results

Table 4-2 summarises the velocities of Lamb wave travelling in the steel plate and CFRP-strengthened steel plate calculated using DISPERSE and FE model respectively. In the steel plate, the wave velocities calculated are very similar because the material properties of steel used in these two methods were identical. The result of FE modelling shows that, with the application of CFRP laminates, the wave velocity increases.

Table 4-2 Comparison of velocities of Lamb wave travelling in steel plate and CFRP-strengthened steel plate

Specimen	DISPERSE	FE model
Steel plate	5170 m/s	5083 m/s
CFRP strengthened steel plate	N/A	5386 m/s

Figure 4-5 shows the actual and calculated crack lengths against the growth of crack for different sensing paths in the sensing network. Figure 4-5 (a) shows the crack length computed using captured signal in path S1-S5. An increment can be seen in the calculated crack length as the crack grows, and the trend and magnitude shows good agreement with the actual crack growth. For sensing paths S1-S6 and S2-S5, the growth of fatigue crack is successfully detected and the growth rate of the calculated crack length is similar to that of the measured length. It is also noted that the sensitivity of the captured signals for crack detection in paths S1-S6 and S2-S5 is less than that of S1-S5, especially at short crack lengths. Figure 4-5 (c) shows the results calculated based on the signal captured in path S2-S4, which is the furthest path away from the crack. The results show that sensing path S2-S4 is incapable of

detecting the fatigue propagation, indicating that the presence of crack in the sensing path, which causes wave scattering, strongly affect the captured transmitted S0 mode. All results calculated using signals captured in each sensing path are weighted based on the interferences of the propagating crack on the propagation of the transmitted signal in the sensing paths. The confidence coefficient of the calculated crack length is weighted as 1 if the length is calculated using the signal captured in sensing path that directly encountered with the crack, otherwise confidence coefficient is weighted as 0. The weighted results are then combined to generate a final result that derived from all sensing paths as a sensor network. Figure 4-6 shows the calculated crack lengths based on information from all sensing paths. The calculated crack lengths show good agreement with the actual ones, in the consideration of the cracking to be quantified is in the order of millimetre.

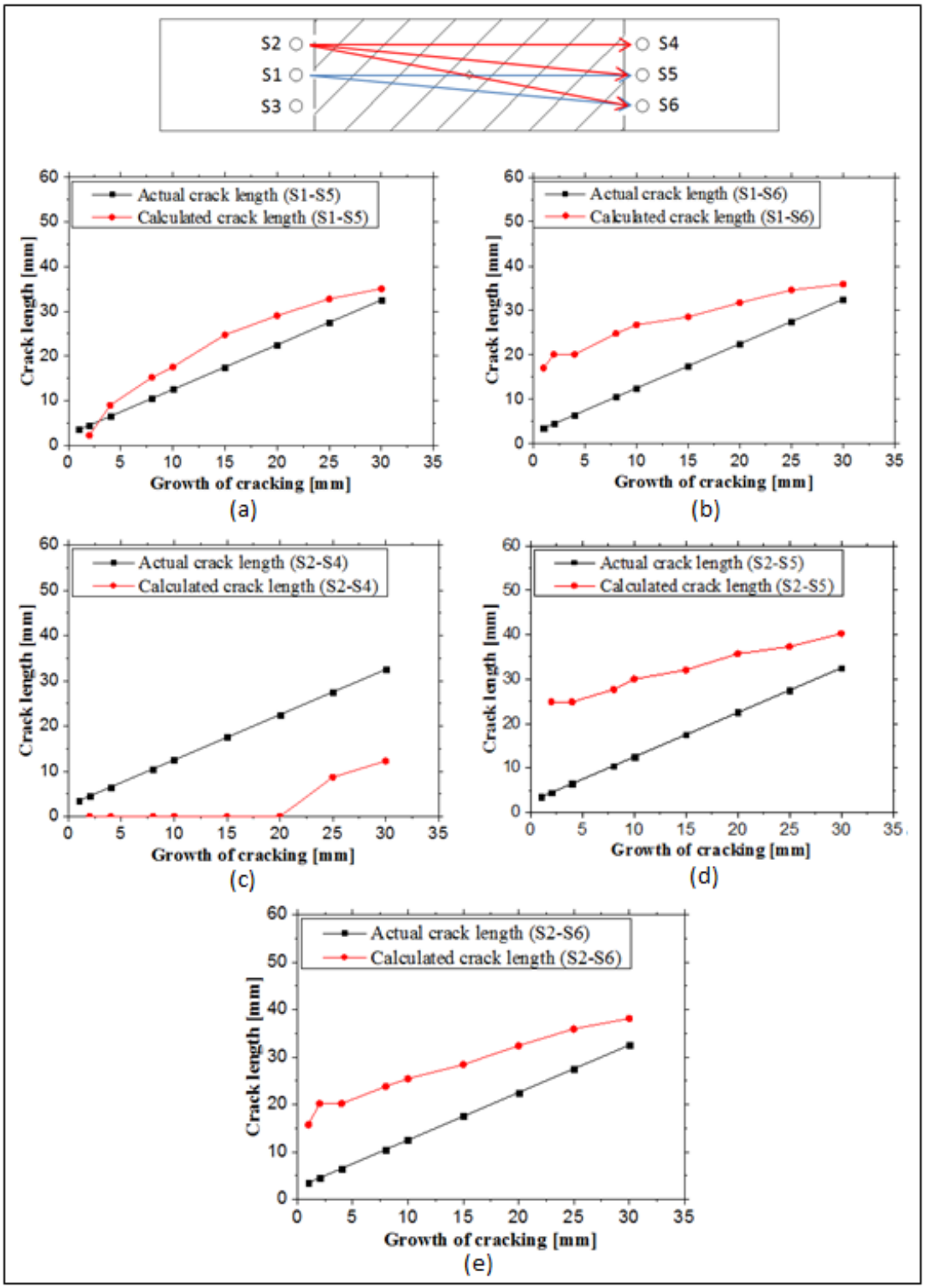

Figure 4-5 Calculated crack lengths (FE) for sensing path a) S1-S5, b) S1-S6, c) S2-S4, d) S2-S5, and e) S2-S6

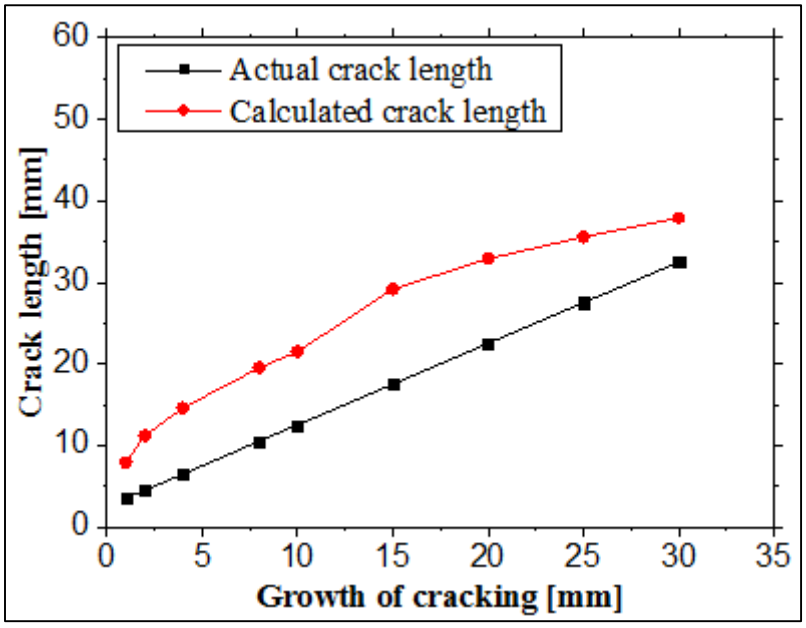

Figure 4-6 Calculated crack length (FE) based on all sensing path within the sensor network

4.3. Experimental analysis

Following the simulation, lab-based experiments have been conducted to validate the proposed methodology. The specimen preparation and experiment set up is the same as mentioned in previous Section 3.6. The same excitation signal as used in simulation is generated with a peak to peak output voltage of 1.2 $V_{p\text{-}p}$, which is then amplified to 120 $V_{p\text{-}p}$ by the Ciprian power amplifier. The signal is applied on one PZT acting as the actuator, and the response signals are acquired by the rest of PZTs through the Tektronix 4034B digital signal oscilloscope with a sampling frequency of 25 MHz after 128 samples averaged.

To facilitate the fatigue crack propagation, the specimen undergoes a high-cycle fatigue testing on an Instron 8802 servo hydraulic testing machine, as shown in Figure 3-15, subject to a sinusoidal tensile load varying from 13.5 to 135 kN, followed by a sinusoidal tensile load varying from 74.25 kNto 135 kN to produce beach marks. The test runs and stops every 66,000 cycles, and

thereby the signals are captured every 66,000 cycles while the specimen remains clamped in the machine to maintain constant boundary condition. After roughly 1.1 million cycles, the specimen is completely failed. Figure 4-7 shows the beach marks left on the cross section of the failed specimen. These marks indicate the actual crack length subject to certain cycle number of fatigue loading. It is noted that only 7 marks are left on the cross section, indicating that beach marking technique is not sensitive to small fatigue cracks at early stage, around 600,000 cycles.

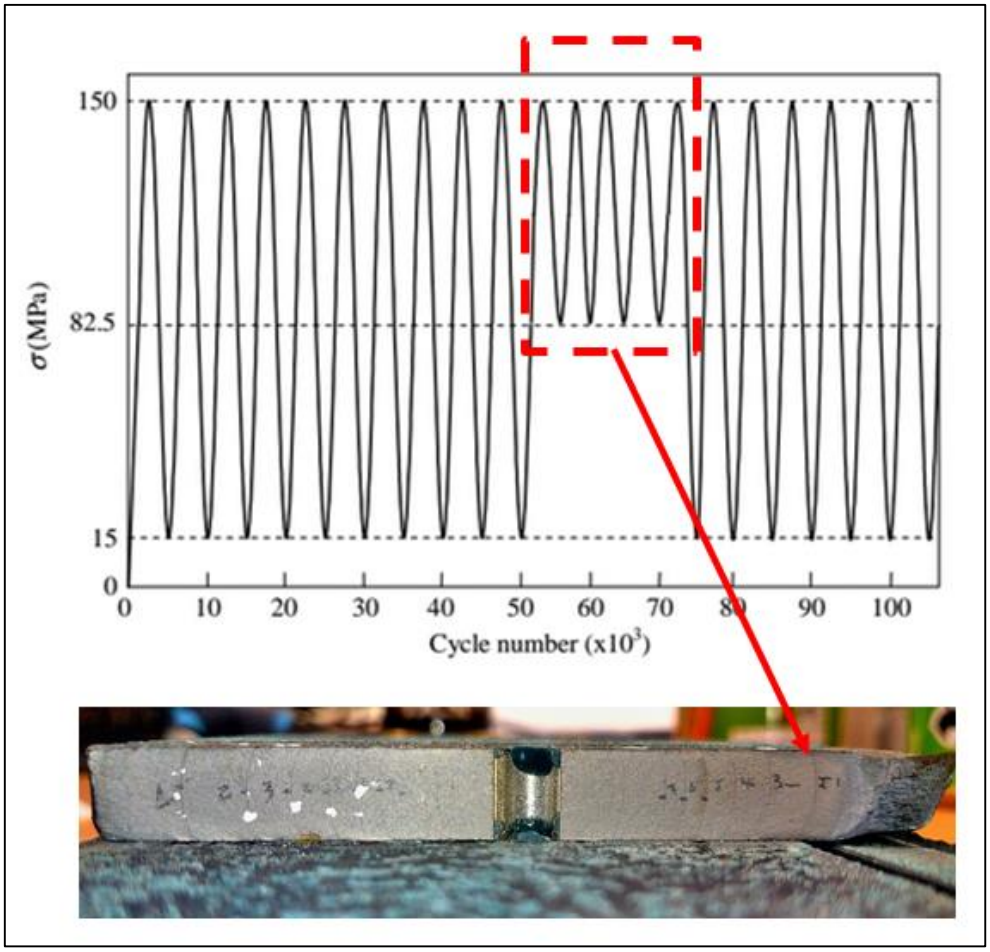

Figure 4-7 Beach marks on failure face of the specimen

4.3.1. De-noising of raw signals

In contrast with the signals generated from numerical modelling, the signals captured through lab-based experiments unavoidably contain a number of

ambient noises in different frequency bands. The damage-scattered signals of interest can be easily masked by these noises, making the feature extraction a challenging task. The first vital step to process the signals is thus de-noising.

Figure 4-8 (a) presents the raw transmitted signal captured in sensing path S1-S5. The black solid line denotes the benchmark signal and the red solid line represents the signal captured after undergoing certain number of fatigue loading with crack developed, denoted as the damage state. It was noted that there were significant differences in these signals, which make them incomparable even though the signals are captured in the same sensing path. There was a clear 5.5-cycle wave in the captured signal at the same time when the signal was activated at the actuator. This is known as cross-talk phenomena, which refers to electromagnetic interference from one channel to another. Since the cross-talk does not interference with the desired wave mode, it can be removed without causing information loss. It was also noted that the captured signals were incline and originated from non-zero amplitude (energy). It is because the strong and low-frequency vibration from the fatigue machine is captured by the PZTs along with the desired transmitted Lamb waves. The captured low-frequency vibration signal was caused by the low-frequency vibration of the fatigue machine when it was operating. As the specimen was clamped in the fatigue machine, it vibrated at a frequency which was same as that of the machine. The surface-mounted PZTs would therefore capture the vibration signal throughout the whole time duration. The amplitude of these vibration signals varied with time following a sine trend. However, comparing to Lamb waves frequency (in kHz), the vibration was at relatively low frequency (in Hz), with longer interval. So for a short time interval, as shown in Figure 4 8

(a), only the very front part of the vibration signal was presented in the figure, hence it only appeared like a linear trend. The frequency profile of typical signal of damage state is obtained using fast fourier transform (FFT), as illustrated in Figure 4-9, where strong low-frequency noise, frequency of interest and noticeable high-frequency noises co-exist. To remove these undesired signals and other forms of environmental noises, a db10 wavelet is employed.

To minimise the computational time, the de-nosing is processed using MATLAB® built-in function db10. The raw signal is decomposed into 10 decomposition levels, as illustrated in Figure 4-10. As shown in Figure 4-11, the signal at the frequency of interest is located at the 7th level, which corresponds to the frequency range between 97.65 kHz to 195.31 kHz. The de-noised benchmark and damage signals are plotted in Figure 4-8 (b), showing more succinct wave signals. As can be seen, there are apparent amplitude drop and ToF delay in the damage signal compared to benchmark. This is because more energy is reflected by the growing crack and the routine for wave propagation is increased due to the presence of damage. Same feature extraction technique is followed to extract the ToFs as that in Section 4.2.

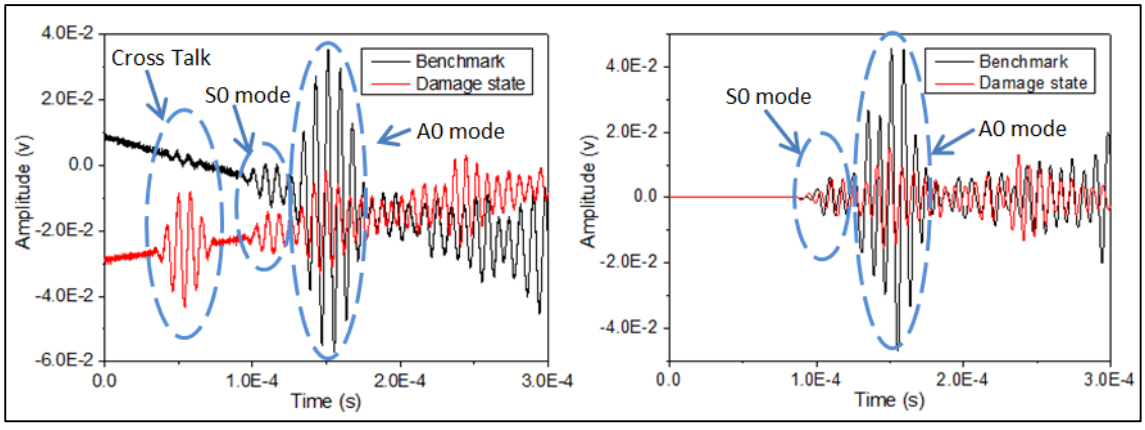

Figure 4-8 Captured signal in path S1-S5 a) original signals, and b) de-noised signals

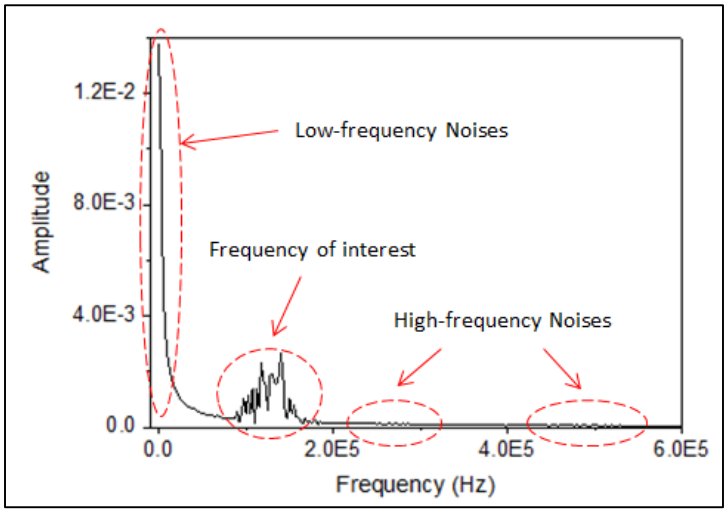

Figure 4-9 Frequency profile of typical signal of damage state

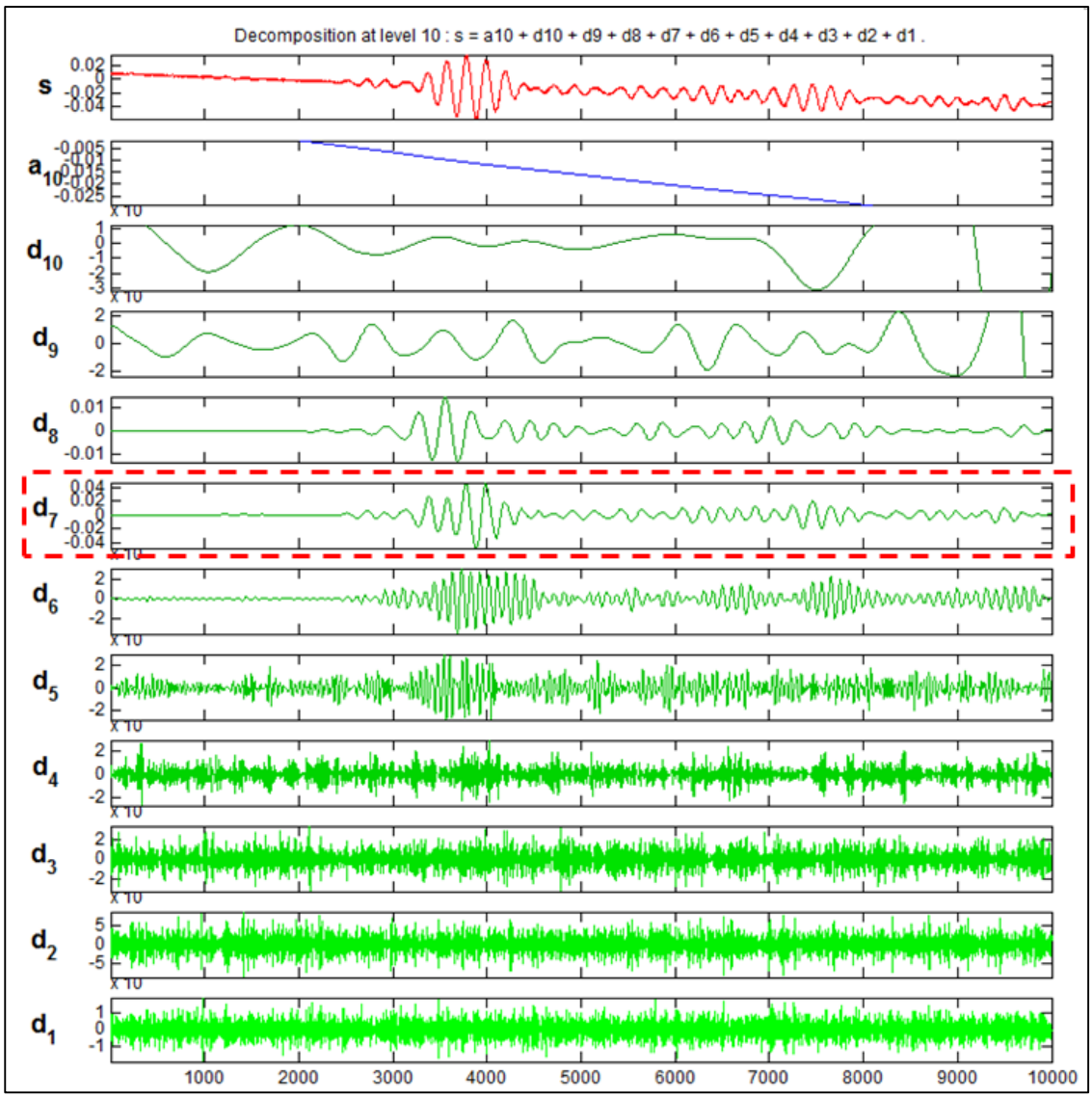

Figure 4-10 Decomposition of raw signal using MATLAB

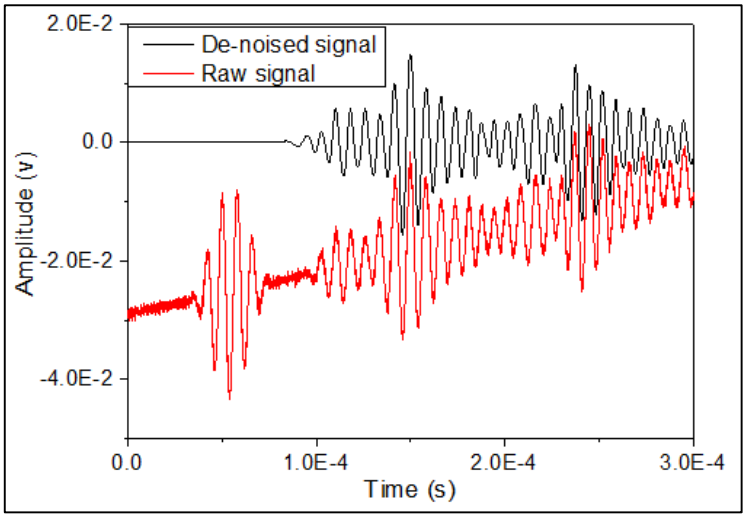

Figure 4-11 Raw signal vs. de-noised signal

4.3.2. Experiment results

Table 4-3 summarises the velocities of Lamb waves travelling in the steel plates and the CFRP-strengthened steel plate calculated using different methods. It is noted that the wave velocity obtained experimentally was much lower than that calculated using DISPERSE and FE model, indicating that the actual material properties, in particular the Young's modulus, were different to those used in the modelling. Nevertheless, the results of the FE and experimental studies showed good agreement that, with the use of CFRP laminate, the wave velocity increased.

Table 4-3 Comparison of velocities of Lamb wave travelling in steel plate and CFRP strengthened steel plate calculated using DISPERSE, FE model and experiment

Specimen	DISPERSE	FE model	Experiment
Steel plate	5170 m/s	5083 m/s	4763 m/s
CFRP strengthened steel plate	N/A	5386 m/s	4836 m/s

The results obtained by proposed damage detection method are shown in Figure 4-12. The black dot line represents the measured length of fatigue crack based on the beach marks left on the failure specimen surface. Due to the strong stiffness of steel plates at the early stage of fatigue process, it is impossible to create beach marks on the failure surface, and thereby crack length cannot be measured against fatigue cycles until the crack length grows to around 12 mm. The red dot line denotes the calculated crack length using the proposed method. Figure 4-12 (b), (e) and (f) show the results of sensing paths S1-S5, S2-S6, and S3-S4 respectively. The signals in these paths are directly interact with the crack since benchmark state. Continuous increments can be observed in these paths, indicating the growth of a crack under fatigue loading. However, the accuracy of crack length detection varies with different paths. The calculated length in S2-S6 shows good agreement with the measured length, while remarkable difference between the calculated and measured length can be observed in path S3-S4. Figure 4-12 (a), (c), (d) and (g) present the crack length in paths when the first arrived S0 mode only interact with the crack of a length larger than 12.5mm, where clear increasing trends in length can be observed. Similar conclusion can therefore be made that the sensitivity of the method to detect crack varies with the signals in different paths. Figure 4-13 shows the crack lengths calculated using signal feature obtained in all sensing paths, indicating that fatigue crack propagation due to cycling loading can be successfully evaluated using Lamb waves.

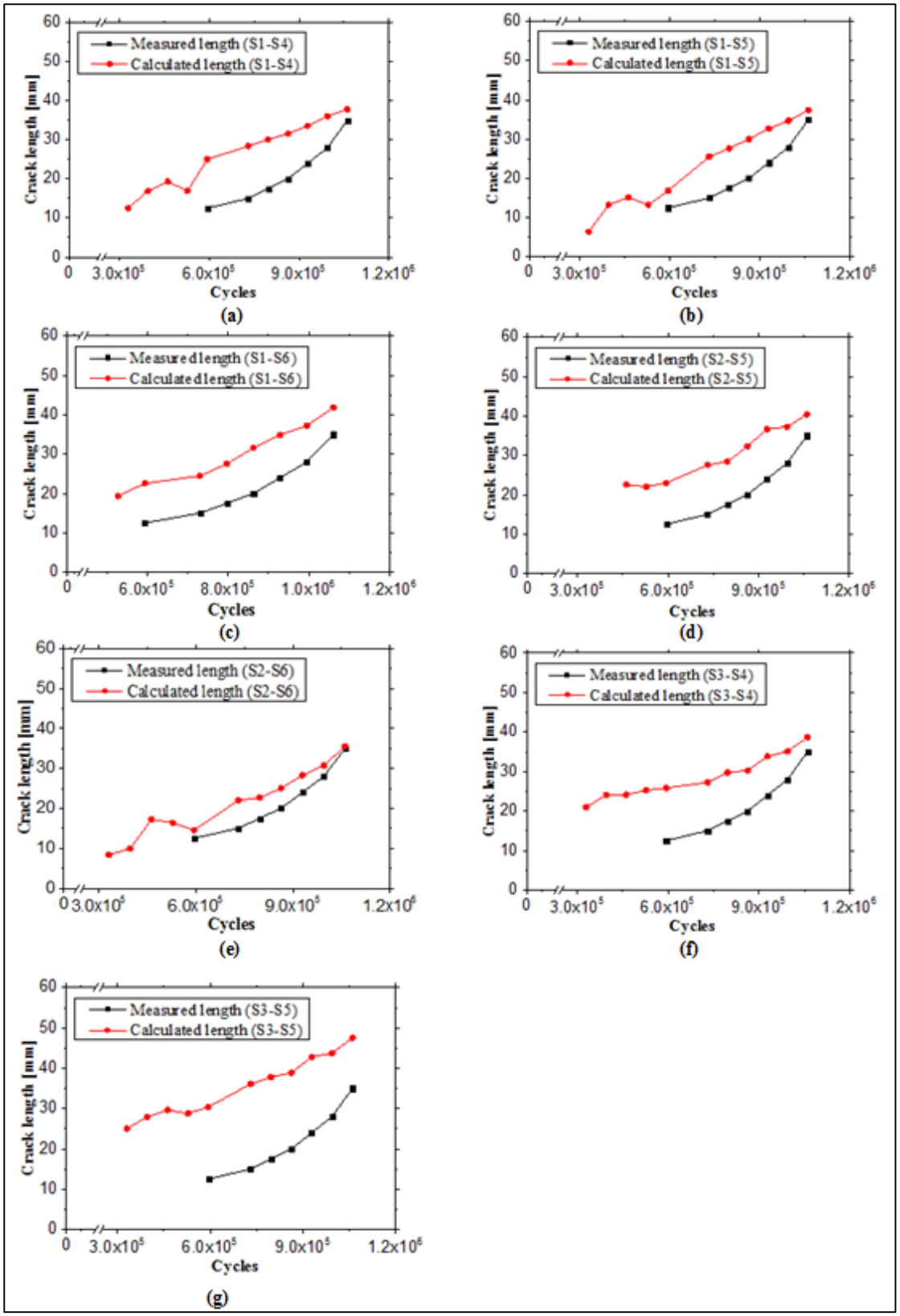

Figure 4-12 Calculated crack lengths (Test 1) for sensing path a) S1-S4, b) S1-S5, c) S1-S6, d) S2-S5, e) S2-S6, f) S3-S4, and G) S3-S5

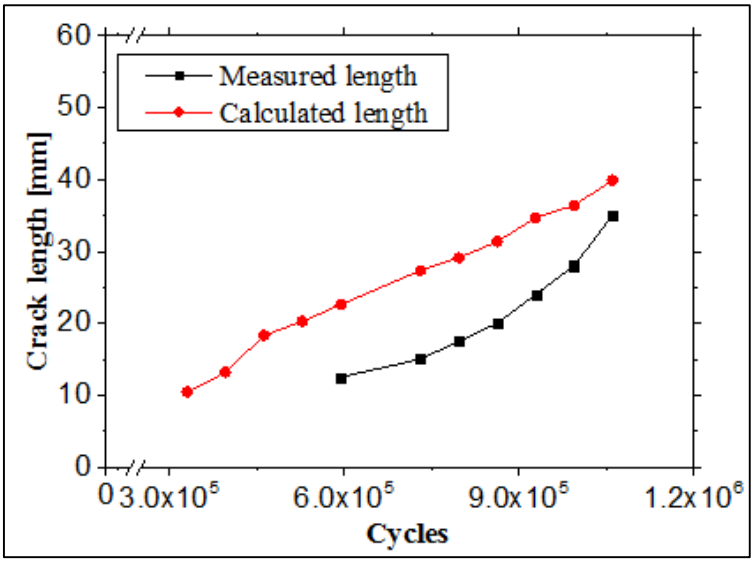

Figure 4-13 Calculated crack length (Experiment) based on all sensing paths within the sensor network

4.4. Summary

FE models and experimental validations were conducted in this chapter to evaluate the feasibility of using low-frequency Lamb waves for the detection of concealed fatigue crack growth. The results showed good correlation between the features of Lamb waves, such as ToF and the propagation of concealed fatigue cracking. The propagation of fatigue crack was successfully detected using the proposed methodology both numerically and experimentally.

The incapability of Lamb waves to detect the initiation of cracking was possibly caused by the larger wavelength (around 38.4mm) at the frequency selected in this study compared to the smaller crack lengths. It was well recognised that half wavelength of a selected wave mode should be shorter than or equal to the damage size to allow the wave to interact with damage. It was also noted that changes in the length of the wave propagation route due to cracking growth were marginal for small-scale crack lengths in current sensor configuration. Even marginal inaccuracy of data processing and feature extraction could

strongly affect the precision of crack length detection. Furthermore, due to the small size and configuration of the specimens used in this study, the locations of transducers in the sensor network were limited, leading to strong interference from waves reflected from boundaries in the first arriving wave package.

Chapter 5. Identification of crack initiation using nonlinear Lamb waves

In this chapter, the proposed nonlinear Lamb wave-based method was employed to identify the crack initiation in both steel plates and CFRP-strengthened steel plates via numerical simulation and experimental validation. Firstly, the excitation frequency that enabled the breathing behaviour was selected. A 3-dimensional steel plate model was simulated to exam the proposed method, and then CFRP laminates were bonded to both surfaces of the steel plate to characterise the effects of CFRP laminates on Lamb waves. Experiments were conducted on both steel plates and CFRP-strengthened steel plates. The numerical and experimental results were presented and discussed.

5.1. Excitation frequency

In contrast to the selection of excitation frequency for linear method, which is focusing on obtaining the maximum amplitude for the captured mode, there exist certain excitation frequencies for a certain specimen at which the fundamental modes are accompanied by a cumulative second harmonics, simultaneously satisfying synchronism and non-zero power flux. Commonly used mode pairs that satisfy both the conditions include (S1, S2), (S2, S4), (S2/A2, S4) and so on. The mode pair used in this study is (S1, S2) because they are the fastest modes at their corresponding frequencies, and thereby they can be easily identified even with the presence of other modes. As illustrated in Figure 3-2, the mode pair (S1, S2), of which S1 at the frequency of 377 kHz and S2 at the frequency of 754 kHz satisfy both the conditions and meet the same phase (5850 m/s) and group (4700 m/s) velocities. Therefore, it is

expected that when S1 mode at 377 kHz is excited in the specimen, the corresponding second harmonic, S2 mode is generated at the twice the excitation frequency.

5.2. Numerical modelling analysis

Two sets of simulations were carried out, (1) 3-D Lamb wave propagation in a pristine plate and (2) 3-D Lamb wave propagation in a damaged plate, to access the feasibility of employing nonlinear Lamb waves to identify the crack initiation. A 3-dimensional steel plate was first simulated schematically according to Figure 3-1 (a), to study the nonlinear Lamb wave characteristics when propagating in single-layered plate. The modelling of material nonlinearities was achieved by introducing material constants including density, Young's modulus, Poisson's ratio and third-order elastic (TOE) constants in the modelling. To simulate the fatigue crack, a 0.5 mm long, through-thickness seam crack was introduced to the end of the notch. A contact pair interaction and associated properties were imposed to the crack interfaces to simulate CAN. A 15.5-cycle Hanning windowed sinusoidal tone burst at 377 kHz was excited by imposing uniform in-plane radial concentrated forces on the nodes along the periphery of the actuator. The excitation frequency of 377 kHz enabled the generation of S1 mode as fundamental wave mode, and thereby induced S2 mode at frequency of 754 kHz, as shown in Figure 3-2. Moreover, the time increment of the calculation was controlled to maintain the simulation stability. Double precision was employed in simulation to ensure calculation accuracy.

5.2.1. Feature extraction and damage identification

To expound the feature extraction method, a typical benchmark signal (undamaged) and a current signal (with 0.5 mm seam) in the time domain acquired in the steel plate model via path S2-S4 are presented in Figure 5-1 (a). As can be seen, these two signals were almost identical in the time domain, indicating that there are no apparent waves scattered by the small-size crack, and thereby unable to identify the location of crack using any ToF. However, it was expected that when S1 mode is excited at 377 kHz in the specimen, S2 mode at twice the frequency could be generated once the wave encounters fatigue crack. To illustrate the existence of second harmonics, these signals were processed through fast Fourier transform to obtain the frequency profile, as shown in Figure 5-1 (b). The energy profiles of these two signals were almost identical at the excitation frequency, indicating there is no apparent energy loss due to damage-scattering. However, a weak but significant energy was observed in the current signal at twice the excitation frequency. This energy came from the damage-induced S2 mode.

In order to extract the useful feature, digital signal filter (DSF) was employed to process these signals. The DSF was designed using MATLAB build-in function *fdatool* as shown in Figure 5-2. A Hanning windowed finite impulse response (FIR) bandpass filter was designed to extract transmitted wave within the frequency range of interest while excluding others. Since the upper and lower threshold of the excitation frequency range was ± 50 kHz from the central frequency, same thresholds were employed to define the frequency band for the DSF, and therefore minimizing the information loss due to the filtering. The thresholds of fundamental frequency were 327 kHz to 427 kHz and the

thresholds for double frequency were 704 kHz to 804 kHz. Furthermore, the specify order of the filter was 100 to produce a more accurate results.

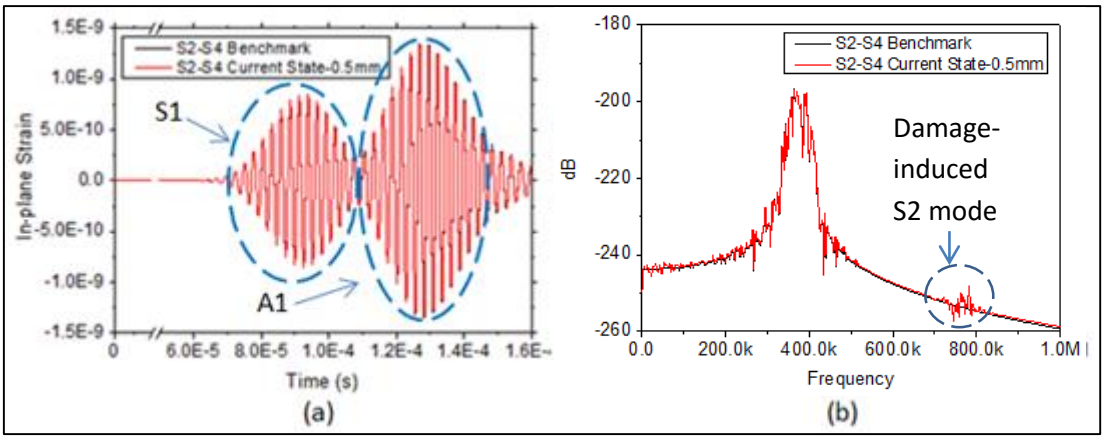

Figure 5-1 (a) Typical benchmark and damage state signals in the time domain (captured via S2-S4) and (b) FFT of the benchmark and current state signal

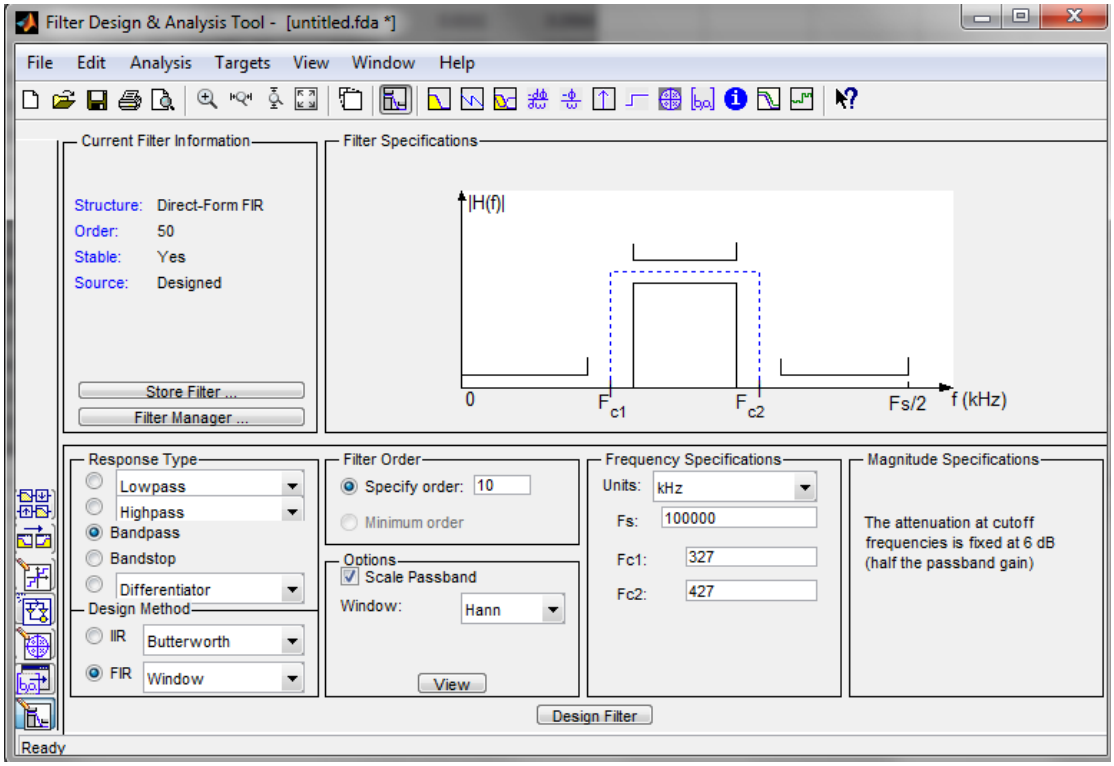

Figure 5-2 Filter design in MATLAB

The wave components at the fundamental and double frequency bands were extracted and plotted as a function of time as shown in Figure 5-3 (a) and (b) respectively. The first hump denoted the first arrived transmitted S1 mode,

followed by the A1 mode. The arrival time of S1 mode was at t_1 in Figure 5-3 (a) The amplitude profiles of the benchmark and damage state signals at the fundamental frequency were almost identical, which further confirmed that that there were no apparent waves scattered by the small-size crack, and therefore unable to identify the location or severity of the crack. As for the wave components at double frequency, it was noted that second harmonics already exist in the benchmark signal. These nonlinearities come from the material nonlinearities of the intact specimen as well as any mathematical nonlinearity from FE program, which were however with marginal amplitudes. The amplitude profile of the damage state signal diverged from the benchmark and increased from t2. This increased amplitude profile came from the CAN introduced in the damage state. It was hence the S2 mode generated when the transmitted S1 mode interacted with the fatigue damage and the t_2 denoted the arrival time of the damage induced S2 mode.

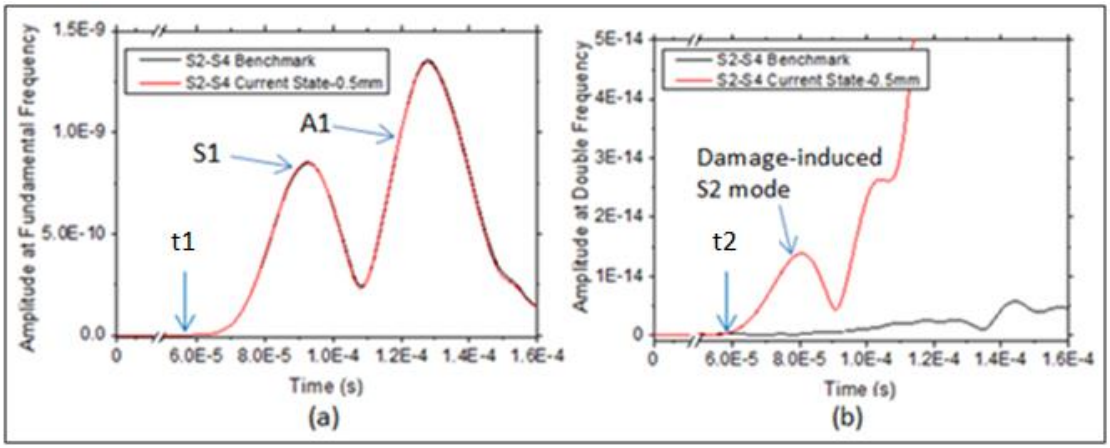

Figure 5-3 (a) the amplitude profiles at the fundamental frequency, where S1 mode is the first arrival mode at time t1 and (b) the amplitude profiles at the double frequency, where damage-induced nonlinearity arrives at t2

With known positions of sensors and ToF of S1 mode, t_1, the group velocity of S1 mode could be calculated. The group velocity of damage-induced S2 mode was expected to the same as that of S1 mode as discuss in Section 3.2.

However, it was observed that the damage-induced S2 mode arrives shortly after the S1 mode, which was due to the longer sensing path caused by the fatigue crack. The length of sensing path that S2 mode travels could therefore be calculated and the relative position of the crack relating to the sensor position could be determined. An elliptical locus could be plotted to denote possible damage locations in term of possibility, as shown in Figure 5-4. Repeating the above procedure for all sensing paths in the sensor network and fusing all the generated elliptical loci, an ultimate image could be produce to highlight the damage location with the highest possibility.

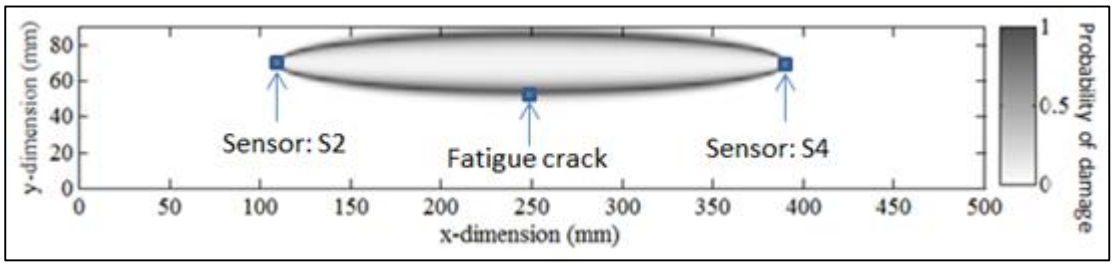

Figure 5-4 an image showing the probability of damage detected via S2-S4 sensing path

As shown in Figure 5-5 (a), the thin black block denoted the approximate location of the fatigue crack which was located at the vicinity of the actual crack tip. A finer diagnostic image, as shown in Figure 5-5 (b), could be generated by multiplying all possible images. The possibility of damage presents at certain location was calculated by multiplying the possibilities detected in each sensing path at that location. The location was only highlighted in the image if the damage was detected by all the sensing paths simultaneously, and excluded all other images even if the location could be detected in certain paths. Hence, it was concluded that the fatigue crack could be successfully highlighted using the proposed nonlinear method numerically.

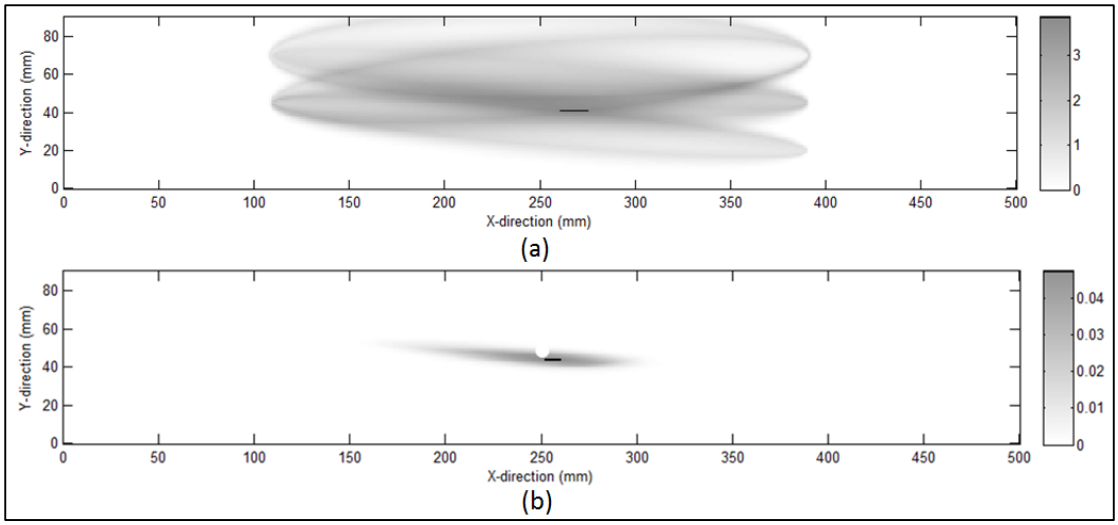

Figure 5-5 Diagnostic image after fusion (a) addition result and (b) product result

5.2.2. Wave-damage interaction when specimen subjected to a constant tensile loading

Since civil infrastructures were subjected to constant dead load (e.g. self-weight) and various live loads, a model containing fatigue cracks and subjected to a constant tensile loading was conducted to simulate the loaded scenario. However, it is difficult to simulate a dynamic loading (Lamb waves) while the model is continuously subject to a constant static loading in the same model. To investigate the loaded scenario, two models were conducted sequentially. The first model was processed through Abaqus Static/General to generate the deformed model, in which the fatigue crack was at open scenario due to the tensile loading. The geometry, material properties and mesh density were same as those in Section 3.1. Pressure at magnitude of 41.25 N/mm^2 was uniformly distributed on both ends of the specimen to simulate the tensile loading applied on the specimen in experiments as shown in Figure 5-6. The model was then processed through Static/General procedure and the deformed model was

obtained, as shown in Figure 5-7, where the fatigue crack was at open scenario and the width of the gap was assumed to be the same as that in experiments under the same tensile loading.

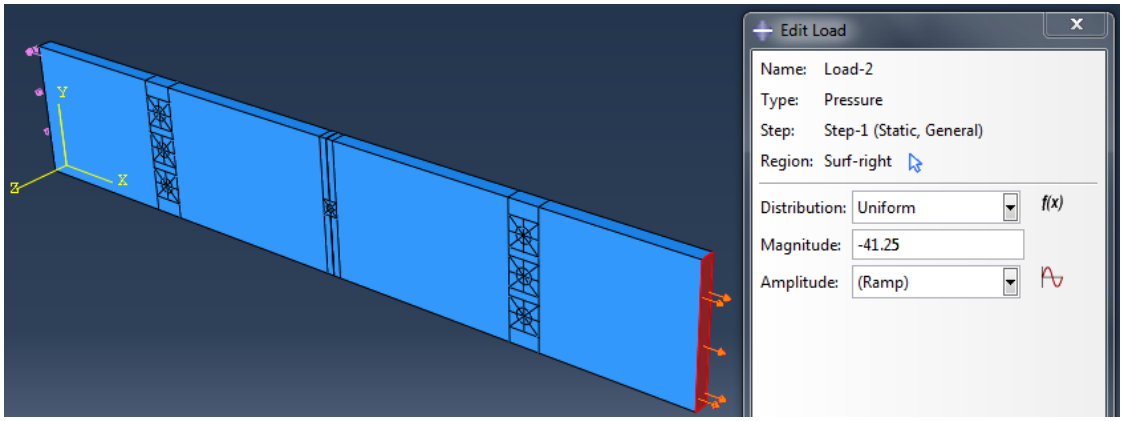

Figure 5-6 Simulation of tensile loading applied on specimen

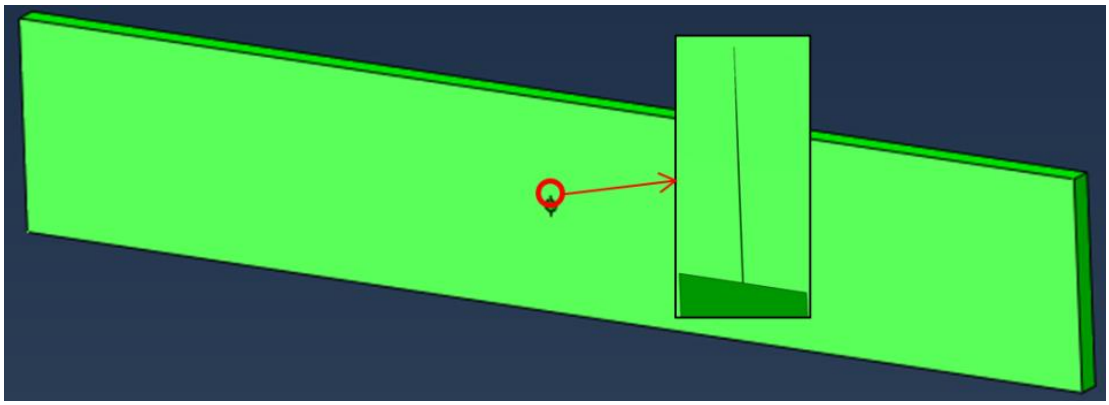

Figure 5-7 Deformed model in which the fatigue crack is in open scenario under tensile loading

As illustrated in Figure 5-8, the deformed configuration at the end of the step of the first model was then imported into Abaqus, and was used as the configuration of the second model, where dynamic/explicit procedure was applied to simulate Lamb wave propagation. By this way, the model was "ideally" subjected to a constant tensile loading, whose effect was shown in the form of deformation. Same modelling procedure as in Section 5.2 was employed to simulate the interaction between Lamb waves and the open crack. The signal feature was extracted using the same method as in Section 5.2.1,

and was compared to that of the signal obtained from the model which was only subject to nonlinear Lamb waves, named the unloaded signal.

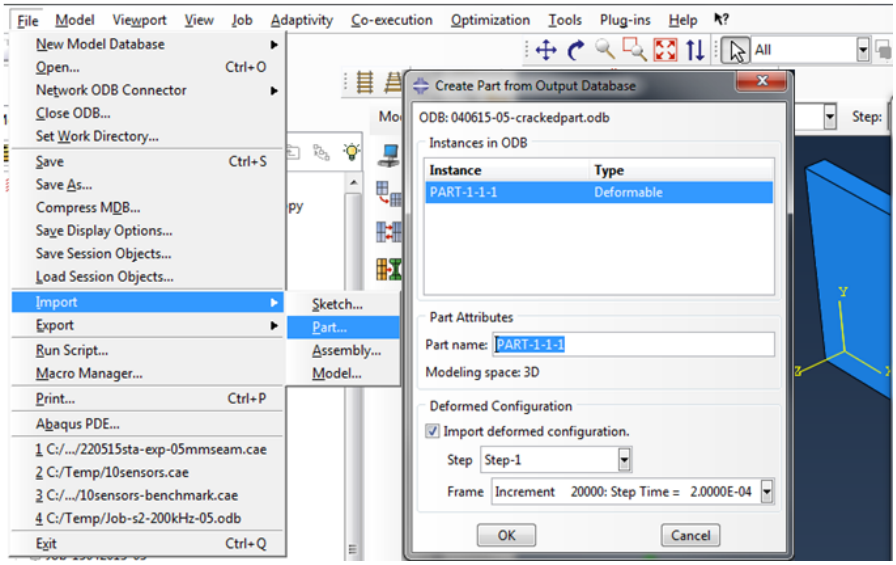

Figure 5-8 Illustration of importing deformed configuration into Abaqus

The amplitude profiles of loaded signal and unloaded signal obtained via sensing path S2-S4 at fundamental frequency and double frequency were illustrated in Figure 5-9. As can be seen, the loaded signal was almost identical to the unloaded signal at fundamental frequency even through the loaded signal was extracted from the model with open cracks. As for the signals at double frequency, large difference between the amplitude profiles of loaded and unloaded signals could be clearly observed, indicating the absence of CAN in the loaded scenario. Figure 5-10 shows the amplitude profiles of loaded signal and benchmark signal obtained via sensing path S2-S4 at fundamental frequency and double frequency, where the signals at double frequency were almost identical. The marginal difference between the two signals was believed to be caused by the material properties and geometry changes. Therefore, it was concluded that no damage-induced nonlinearity can be generated if the

specimen was subjected to a constant tensile loading which could open the fatigue crack and therefore diminished the effect of CAN.

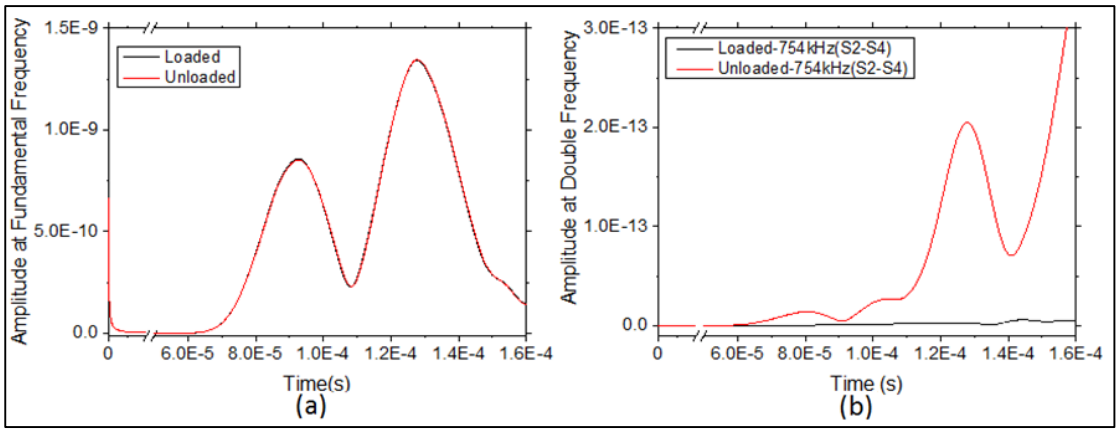

Figure 5-9 Amplitude profiles of loaded signal and unloaded at (a) fundamental frequency and (b) double frequency

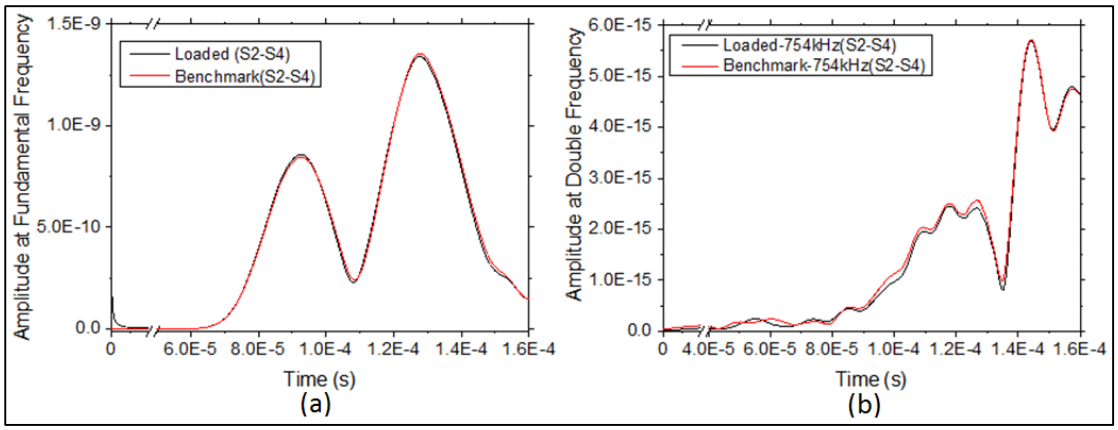

Figure 5-10 Amplitude profile of loaded signal and benchmark signal at (a) fundamental frequency and (b) double frequency

5.2.3. Wave-damage interaction in CFRP-strengthened steel plates

A CFRP-strengthened steel plate model was simulated to study the effects of bonding CFRP laminates to steel plate on the propagation of nonlinear Lamb waves, and to assess the feasibility of using nonlinear Lamb waves to identify the initiation of concealed fatigue crack in the CFRP-strengthened steel plate. To minimise the possible effects on the wave propagation from the computational differences such as model geometry change and difference

mesh, as illustrated in Figure 5-11 and Figure 5-12, CFRP laminates were modelled and tied to both sides of the steel models simulated in Section 5.2. The geometry and material properties of CFRP laminates were same as those in Section 4.2. A 15.5-cycle Hanning windowed sinusoidal tone burst at 377 kHz was excited by imposing uniform in-plane radial concentrated forces on the nodes along the periphery of the actuator. The time increment of the calculation was controlled to maintain the simulation stability. Double precision was employed in simulation to ensure calculation accuracy. By this way, the variables in this model could be controlled, and if there was any change in the wave propagation, it could only be caused by the bonded CRFP laminates.

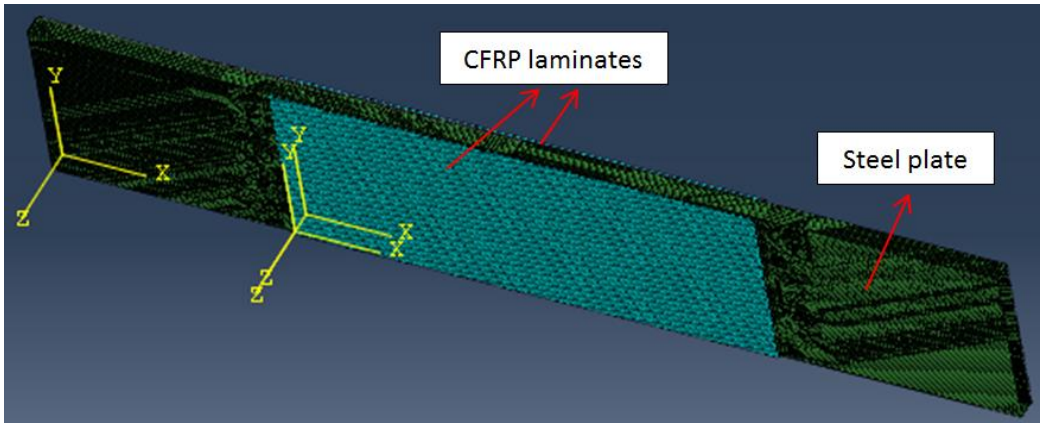

Figure 5-11 CFRP strengthened steel plate model

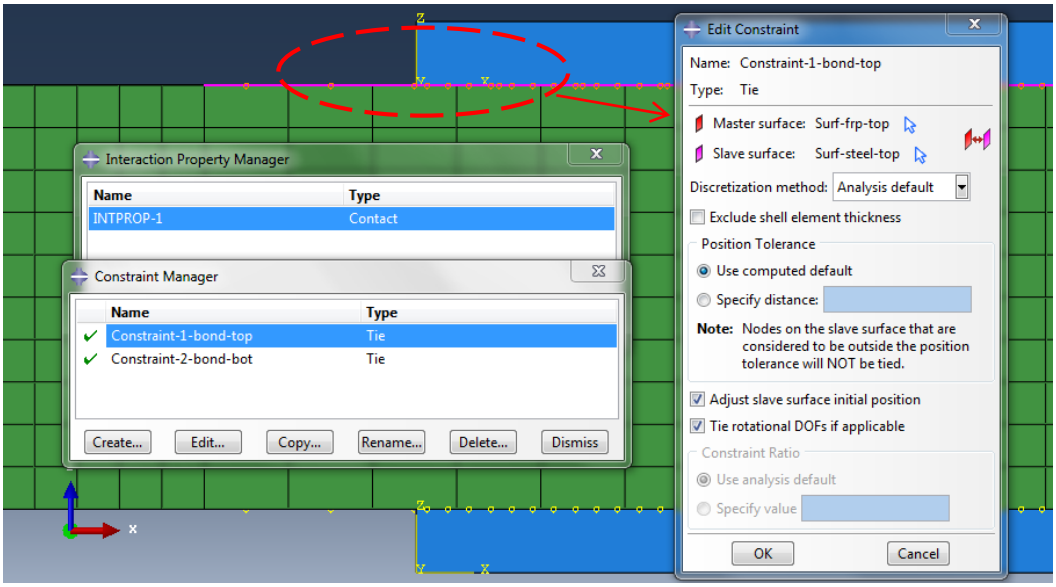

Figure 5-12 CFRP-steel constraint in Abaqus

5.2.3.1. Comparison of signals captured in steel plate and CFRP strengthened steel plates

To illustrate the effects of applying CFRP on steel plates in term of wave propagation, typical benchmark signals captured in the steel plates and the CFRP-strengthened steel plates via sensing path S2-S4 were compared as shown in Figure 5-13. The black solid line represented the benchmark signal captured in the steel plat, while the red solid line denoted the benchmark signal captured in the CFRP-strengthened steel plate. As can be seen, there was a significant amplitude drop in the signal when CFRP laminates were implemented on the steel plate, indicating strong signal attenuation when wave propagated in CFRP laminates. It was also noted that the arrival time of signal captured in model with CFRP is earlier than that in the steel plate, while the arrival time of the peak of the signals were almost identical, indicating that Lamb waves experienced stronger dispersion in CFRP plate but the wave group velocity almost remained constant.

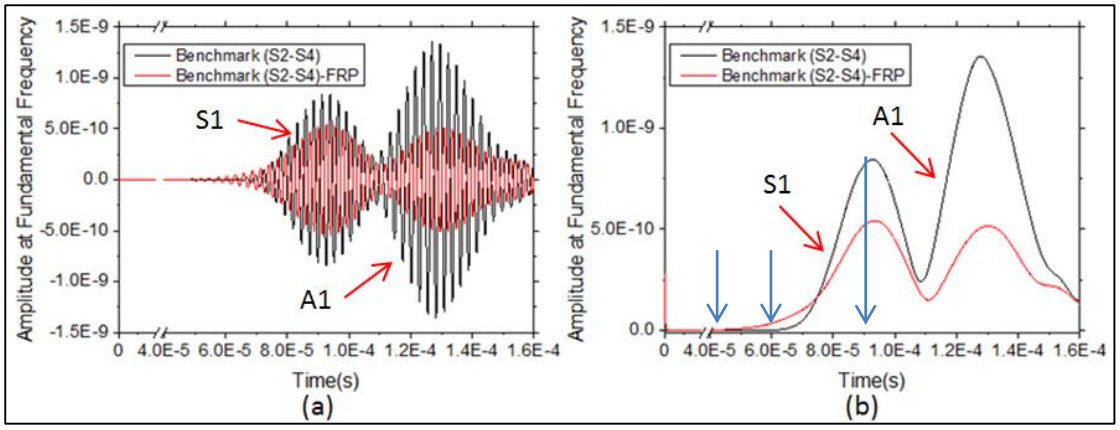

Figure 5-13 Typical benchmark signals captured in steel plate and CFRP strengthened steel plate via sensing path S2-S4 (a) waveform in time-domain and (b) amplitude profile in time-domain.

The captured signals were processed through the digital signal filter designed in Section 5.2.1. The wave components at double frequency were generated and then compared with those captured in the steel plate. As illustrated in Figure 5-14 (a), the amplitude profile of the wave components at double frequency, by contrast, dropped significantly in the CFRP-strengthened steel plate. An amplitude drop in the first arrived damage-induced S2 mode could be observed in Figure 5-14 (b). It was also noted that the arrival time of damage-induced S2 mode in the CFRP-strengthened plate was almost identical to that in the steel plate. It was concluded that when the Lamb wave propagates in the multiple-layered model, the wave components which travel in the steel layer interacted with the fatigue crack, and thereby the damage-induced S2 mode was generated, which propagated in the steel layer to the sensor. Since the damage-induced S2 mode only propagated in steel plate even with the existence of CFRP laminates, the ToF of transmitted signals in both steel plates and CFRP-strengthened steel plate were identical.

Based on these observations, it is concluded that CFRP laminate enhances attenuation and dispersion characteristics of both linear and nonlinear Lamb

waves, and therefore it is believed that the amplitude of Lamb waves get weaker as longer or thicker CFRP laminates applied.

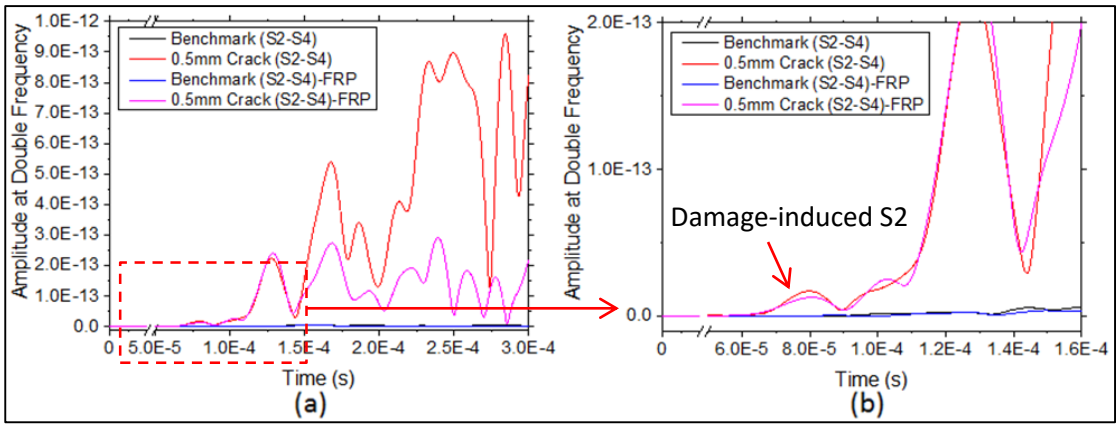

Figure 5-14 (a) Benchmark and damage signals in steel and CFRP strengthened steel plate via sensing path S2-S4, and (b) zoom-in of Figure 5-14 (a)

5.3. Experimental analysis

Lab-based experiments have been conducted to validate the proposed nonlinear methodology. Two sets of specimens, steel plates and CFRP-strengthened steel plates, were tested using Instron 8802 servo hydraulic testing machine to create fatigue cracks, and then inspected by nonlinear Lamb wave-based SHM method. All specimens were prepared following the procedure in Section 3.6.1. 10 PZT sensors were surface-mounted on the steel plates, as shown in Figure 5-15, which formed 50 transmitted sensing paths. These PZTs were placed 15 cm centre-to-centre (5 cm edge-to-edge). For CRFP strengthened steel plates, 6 PZTs were bonded to the surface of the plates at 25 cm centre-to-centre spacing, forming 18 sensing paths.

The excitation signal was a 15.5-cycle Hanning windowed tune burst with a peak-to-peak output voltage of 6 $V_{p\text{-}p}$, which was then amplified to 600 $V_{p\text{-}p}$ by the Ciprian power amplifier. Large amplitude of voltage ensured the responses

of the excited signal being large enough to trigger the breathing behaviour upon interacting with fatigue cracks. An excitation frequency of 377 kHz was used and four modes, A0, S0, A1 and S1, co-existed in the received signal at this frequency, and damage-induced S2 mode was expected to exist at double frequency. The excited signal was applied on one PZT acting as the actuator, and the responses signals were acquired by the rest of PZTs through the Tektronix 4034B digital signal oscilloscope with a sampling frequency of 25 MHz after 128 samples averaged.

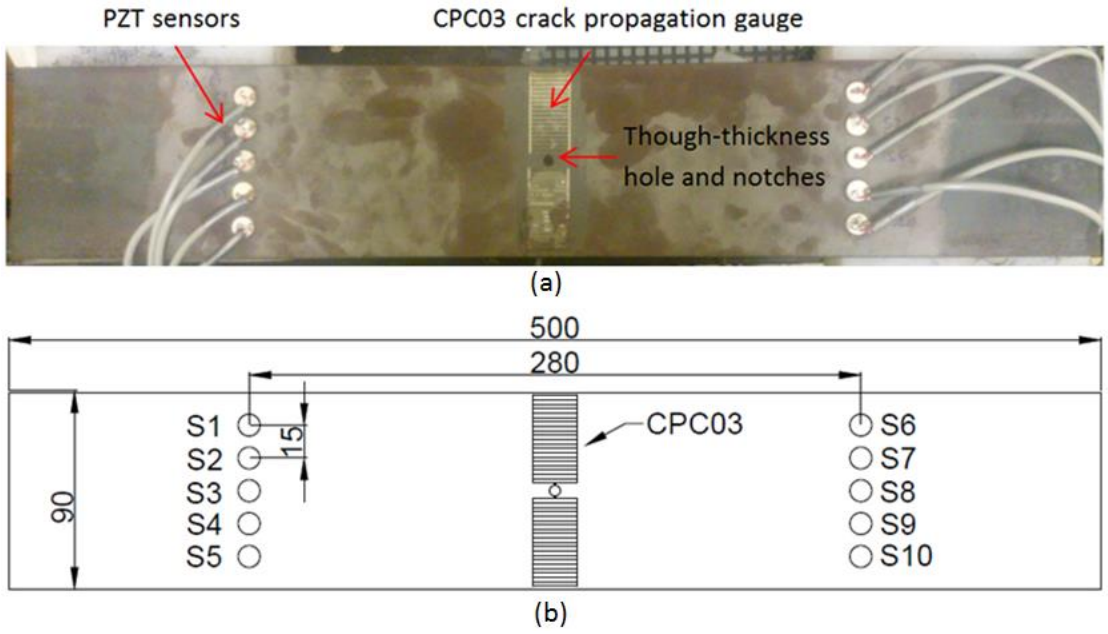

Figure 5-15 (a) Steel plate specimen with 10 surface-mounted PZT sensors and (b) configuration of steel plate

5.3.1. Measurements of fatigue crack size

The fatigue tests were carried out at Monash University Civil Lab. All specimens were subjected to a sinusoidal tensile load varying from 13.5 and 135 kN with a frequency of 20 Hz. In order to monitor and to control the size of the fatigue cracks, CPC03 crack propagation gauges manufactured by Micro-Measurements® were adopted in this study. The detailed dimensions of the

gauge are shown in Figure 5-16 (a) and crack propagation direction is shown in Figure 5-16 (b). The gauge is 0.043 mm thick and consists of 20 resistor strands connected in parallel at a centre-to-centre spacing of 2.03 mm. When mounted to the specimen surface, the resister strands fracture with crack propagation, thereby the crack length can be monitored every 2.03 mm increment and the corresponding cycles of fatigue testing can be recorded. M-Bond 610 adhesive was used to bond the gauge to the specimen surface according to the manufacturer's instruction and the attached crack propagation gauge is shown in Figure 5-17.

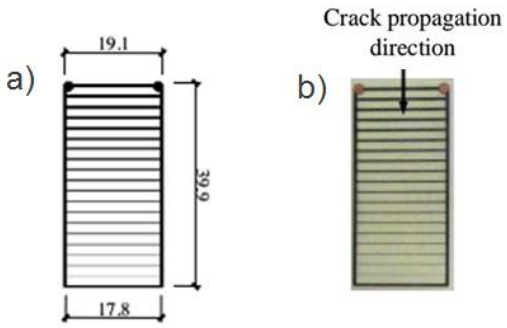

Figure 5-16 a) configuration of CPC03 crack propagation gauge b) CPC03 crack propagation gauge and crack propagation direction.

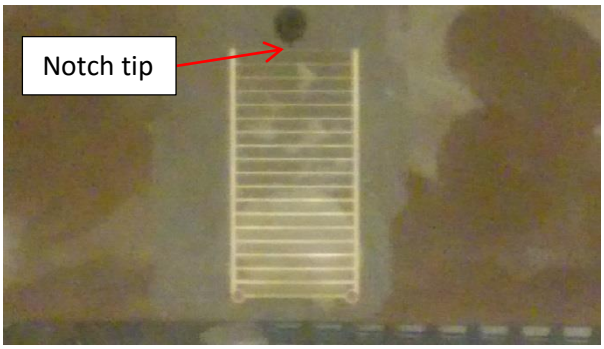

Figure 5-17 Crack propagation gauge bonded to the specimen surface

For the CFRP-strengthened steel plates, due to the presence of CFRP laminates, it was impossible to access the cracked zone, making the

measurement of the crack size a challenging task. In order to generate a fatigue crack and to minimise the created crack size, the specimen was tested and paused every 10,000 cycles increments, and then the signal captured in sensing path, which is directly encountered with the crack, was monitored and compared to the benchmark signal until these signals begin to diverse. In this way, a small-scale fatigue crack could be created.

5.3.2. Experimental results

5.3.2.1. Steel plate

The steel plate was subjected to cyclic loading and the test was paused every 10,000 cycles to check the generation of fatigue crack. After about 120,000 cycles, a 2 mm long crack appeared on the surface of both crack propagation gauge bonded on the specimen, as shown in Figure 5-18.

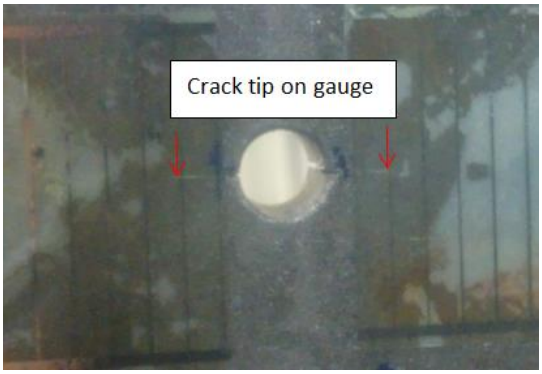

Figure 5-18 Crack on crack propagation gauge

Figure 5-19 (a) shows the benchmark signal and damaged signal in the time domain acquired in the steel plate via sensing path S1-S6, which was the furthest sensing path from the fatigue crack. As can be seen, the first arrived S1 modes in both signals were almost identical. The first several cycles of A_1 mode in both signals were also identical, but the waveforms started to differentiate after that. Figure 5-19 (b) presents the benchmark signal and

damaged signal in the frequency domain. It was noted that at double the excitation frequency, energy profile of cracked signal was stronger than that in benchmark signal, which indicated the generation of damage-induced S2 mode due to the wave-crack interaction. However, a strong 2nd harmonic already existed in the benchmark signal. These nonlinearities may come from the material and geometric nonlinearities of the intact specimen, as well as inherent nonlinearity from the system.

In order to obtain the information of the 2nd harmonic in the time domain, the signals were processed using the digital signal filter designed in previous section. The 2nd harmonics of benchmark and cracked signal are presented in Figure 5-20. As can be seen, there were strong nonlinearities existing in the benchmark signal, even before the transmitted signals arrived sensor S6. This inherent nonlinearity generated from electric instruments strongly and negatively influenced the experimental results, which made it difficult to distinguish between the damage-induced nonlinearity and the inherent nonlinearly from the system. Due to the limitations and availability of electric instruments used in this study, these nonlinearities unavoidably existed in the captured signals, which complicated the determination of the arrival time of the damage-induced S2 mode, and thereby made the accurate detection of crack location a challenging task.

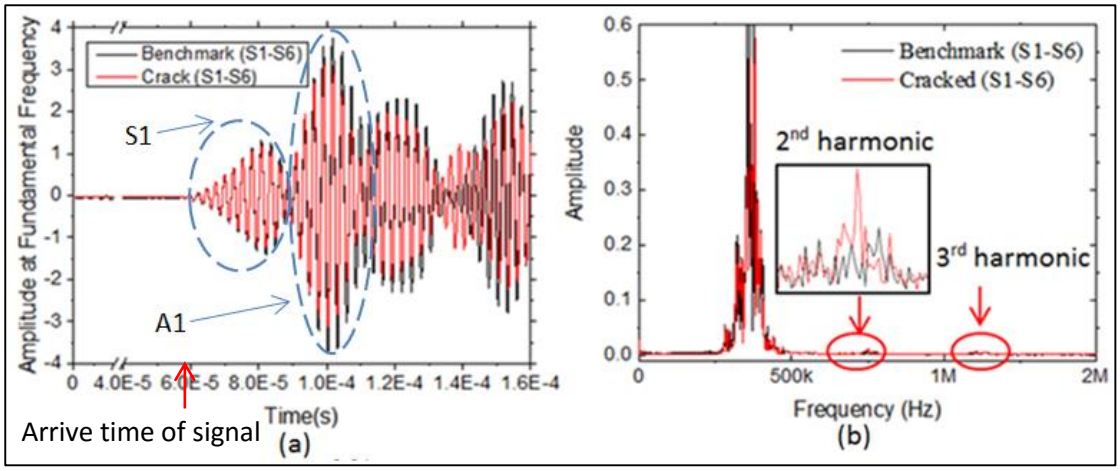

Figure 5-19 Benchmark and crack signal captured in path S1-S6 in (a) time-domain and (b) frequency domain

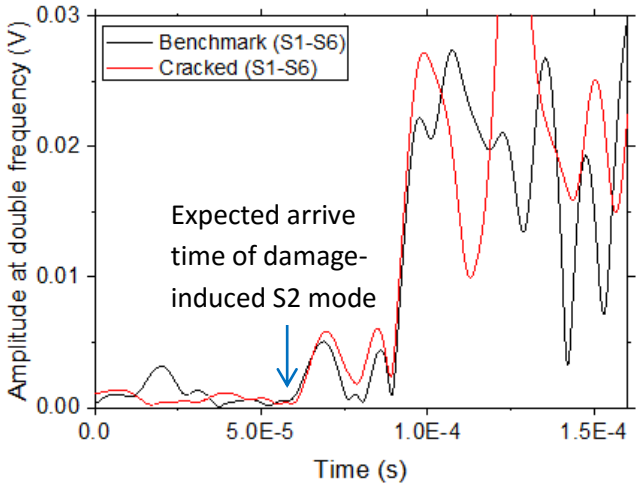

Figure 5-20 Benchmark and cracked signal at double frequency in time domain

Figure 5-21 shows the amplitude profiles of benchmark and cracked signal at double frequency captured via other sensing paths. It was noted that strong nonlinearities exited in all benchmark signals and their waveforms and strengths vary with sensing paths. Even though the damage-induced nonlinearity could be clearly observed in all figures, the determination of ToF of the damage-induced S2 mode remained a challenging task due to the presence of strong nonlinearities in benchmark signals. It was also noted that, nonlinearity of signal is getting weaker while the sensing path is further away

from the crack. As can be seen in Figure 5-22, the nonlinearity of signal captured in S1-S6 was much weaker than that captured in S3-S8, which indicated strong and fast attenuation of damage-induced nonlinearity when travelling in steel plate.

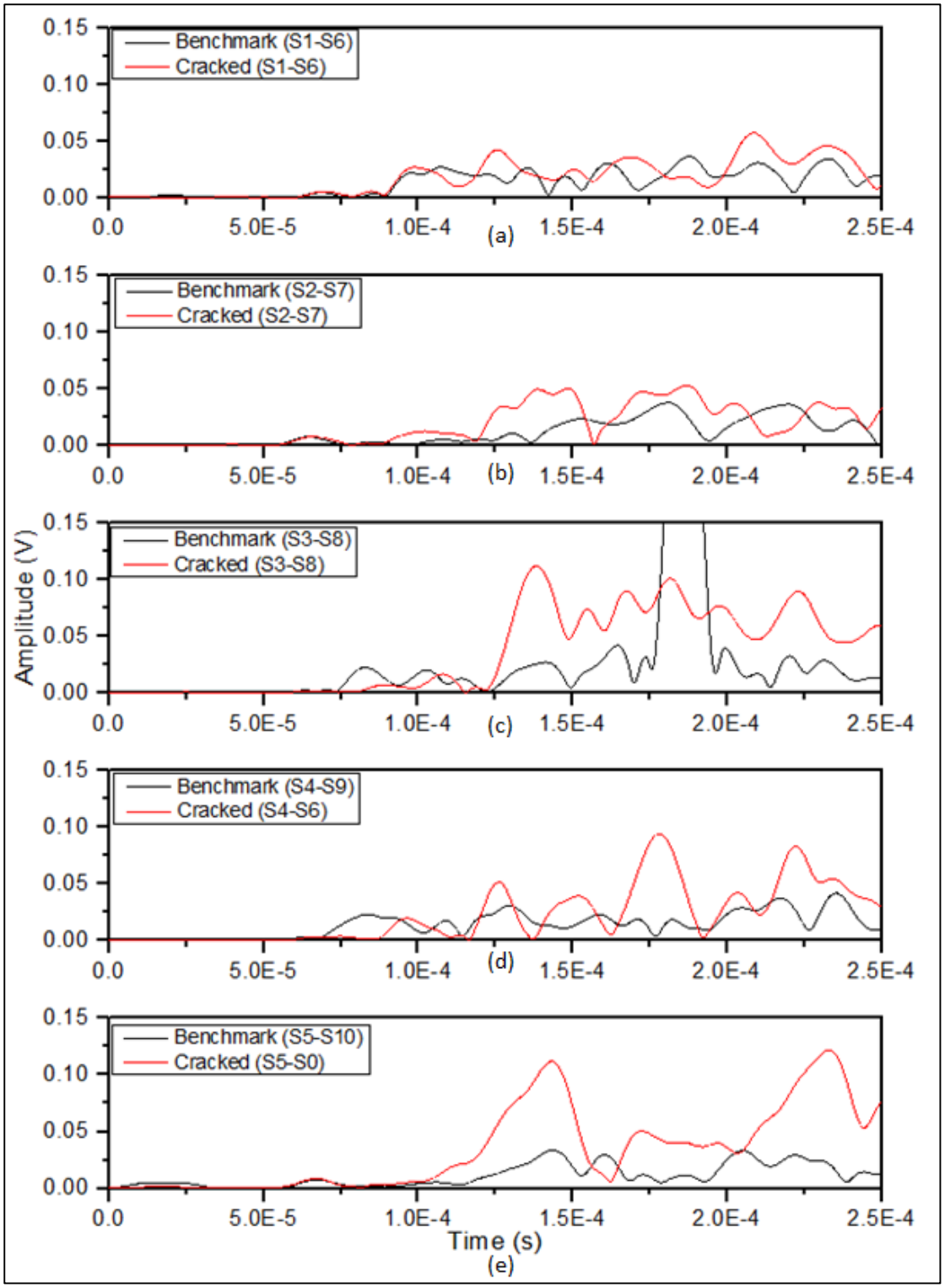

Figure 5-21 Energy profiles of benchmark and cracked signals at double frequency captured via sensing path (a) S1-S6, (b) S2-S7, (c) S3-S8, (d) S4-S9, and (e) S5-S10.

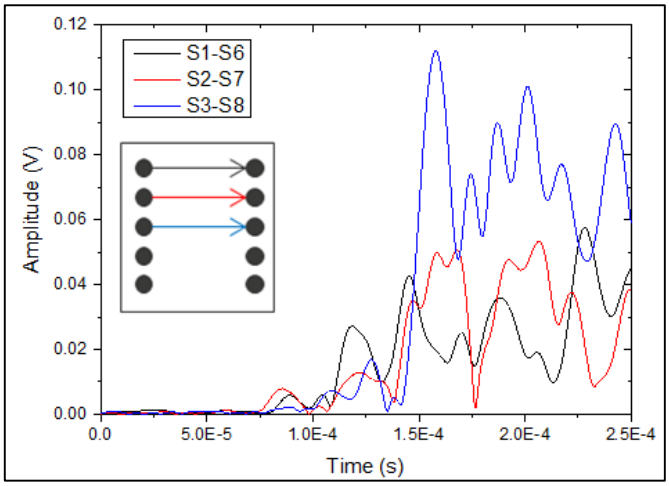

Figure 5-22 energy profile of crack signals at double frequency captured in sensing path S1-S6, S2-S7, and S3-S8

5.3.2.2. CFRP-strengthened steel plate

The experiment was carried out using the same loading range as that of steel plates. After about 280,000 cycles, the signal in sensing path S2-S5 began to deviate from the benchmark signal. Figure 5-23 (a) presents the benchmark signal and the signal captured after 280,000 cycles. There was a small but noticeable difference between these signals, which indicated that a small-scale fatigue crack is generated.

Figure 5-23 (b) shows the energy profiles of benchmark and cracked signal captured via S2-S5 at double frequency. It was noted that the amplitude of nonlinearity of the crack signal is larger than that of benchmark signal. This increment part came from the damage-induced nonlinearity, indicating the generation of fatigue crack.

It was also noted that the amplitudes of both linear and nonlinear signals captured in CFRP strengthened steel plate were much smaller than those captured in steel plate, even though the excitation signal were same, which

mainly contributed to the fact that the signals experience strong attenuation when travelling in CFRP laminate.

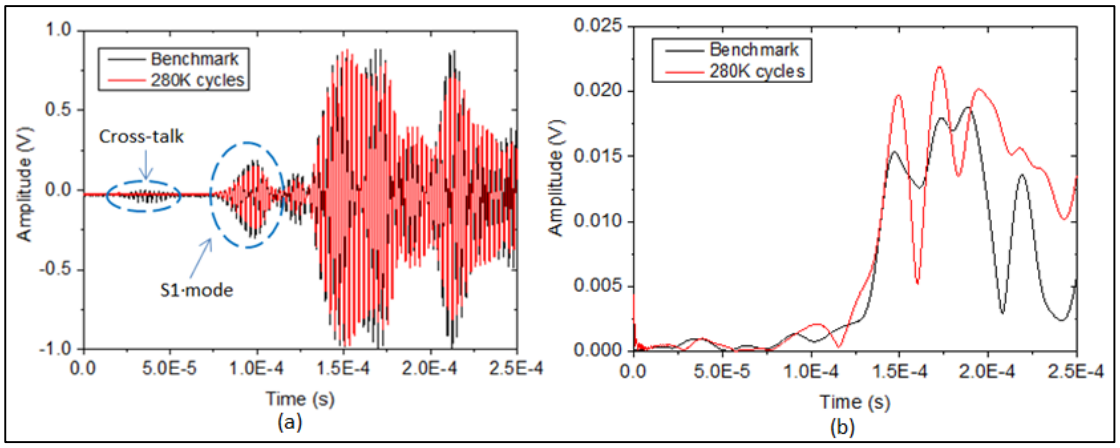

Figure 5-23 (a) captured benchmark and cracked signal in time domain via S2-S5 and (b) energy profile of benchmark and cracked signal at double frequency

5.4. Summary

In this chapter, numerical simulation and experimental study were conducted in order to detect fatigue initiation (small-scale fatigue crack) using the proposed nonlinear methodology. First, a steel plate was used as proof of concept to validate the feasibility of the proposed methodology. Second, a multi-layered CFRP-strengthened steel plate was used to understand the effects of CFRP on nonlinear Lamb waves. Simulation results showed that the proposed methodology could successfully detect the small-scale (0.5 mm) fatigue crack and the energy of both transmitted waves and damage-induced nonlinearity decreased when CFRP laminates were employed. Strong non-damage related nonlinearities were observed in experiments, which made the determination of crack location and severity a challenging task. However, the presence of fatigue damage could be successfully indicated, and the energy of damage-induced nonlinearity was found to be weaker when the signal is

captured in the sensing path further away from the crack. Experimental results also confirmed that both linear and nonlinear Lamb waves experienced strong attenuation when travelling in CFRP-strengthened steel plates.

Chapter 6. Conclusions and recommendations

6.1. Conclusion

This thesis presented numerical and experimental studies of Lamb wave-based SHM for fatigue crack detection in CFRP-strengthened steel plates. One of the main objectives of this research is to evaluate the linear Lamb wave-based SHM method for monitoring fatigue crack propagation in CFRP strengthened steel plates. Another main objective is to evaluate the nonlinear Lamb wave-based method for fatigue crack initiation detection. The effects of CFRP on the characteristics of Lamb waves were presented. The results and conclusions were determined from numerical and experimental studies and presented below.

The principle of the Lamb wave-based methodology for fatigue crack propagation monitoring was described. The dispersion characteristics of Lamb waves were discussed and dispersion curves were generated using DISPERSE®. Phase velocities were used to determine the cut-off frequency before higher order modes were generated and the group velocities were used to identify the wave modes in the captured signals. Experiment study has been conducted on a pristine CFRP-strengthened steel plate to determine the optimal excitation frequency with the strongest signal amplitude. 3-dimensional numerical simulations and experimental validation were conducted to evaluate the feasibility of using linear Lamb waves to detect the concealed fatigue crack growth in CFRP-strengthened steel plates. The results showed good correlation between the features of Lamb waves, ToF in particular in this study, and the length of fatigue crack in both numerical and experimental studies,

which indicated that the proposed method could successfully monitor the concealed fatigue crack propagation. The results also indicated that the relative location of the crack to the sensing paths strongly affected the ability of Lamb waves for the detection of crack growth, i.e. the further the sensing path away from the crack, the less capable the Lamb waves to detect the crack. It was also found that the proposed linear method was incapable to detect the crack initiation or small-scale cracks, and the possible causes were discussed. To overcome these deficiencies, a nonlinear Lamb wave method was proposed to detect the initiation of fatigue crack.

In order to generate significant and cumulative 2^{nd} harmonics, the excitation frequency must be selected deliberately. The mode pair must satisfy the condition of synchronism and non-zero power flux simultaneously. This has been achieved by S1 mode at frequency of 377 kHz, which induced S2 mode at frequency of 754 kHz upon encountered with fatigue damage. This mode pair propagated at same phase and group velocities. First, 3-dimensional simulation of wave propagation in steel plates was conducted to assess the proposed method. The results showed that the initiation of fatigue crack could be successfully indicated and the location of the crack could be determined. CFRP laminates were then bonded to both surfaces of the steel plate to assess the effects of the presence of CFRP on Lamb wave characteristics. The signals generated in the steel plate with and without CFRP laminates were compared and it was found that Lamb waves experienced strong attenuation and dispersion when travelling in CFRP laminates. Lab-based experiments were then conducted to evaluate the efficiency of nonlinear Lamb waves in detection of fatigue crack initiation in steel plates. Results showed that the initiation of

fatigue crack in the steel plate could be successfully indicated. However, strong inherent nonlinearity from instruments was observed in both benchmark and damaged signals in experiments, making the detection of crack location a challenging task. It was also found that the wave nonlinearity captured in sensing path which directly encountered with the crack was stronger than that captured in sensing path which was away from the crack. The CFRP-strengthened steel plates were subsequently tested. The initiation of fatigue crack could be successfully indicated by evaluating the nonlinearities of the signals. However, results showed that the nonlinearities generated in CFRP-strengthened steel plates were much weaker than those in steel plates, indicating that damage-induced nonlinear Lamb waves experienced much stronger attenuation and dispersion in CFRP-strengthened steel plates even though the excitation signal was the same as that used in steel plates.

This study analytically models the propagation characteristics of both linear and nonlinear Lamb waves and the interaction of Lamb waves and defects. Methodologies are developed based on the numerical results, allowing the implementation of Lamb wave-based SHM technique in a lab-based experimental study. The main contributions of this dissertation to the research community are given below.

- Reliable models for linear and nonlinear Lamb wave excitation and collection by circular PZTs in single-layered isotropic structures and multiple-layered structures were developed and were extensively validated with numerical results. The models were simulated using Abaqus/Explicit. The multimodal nature and attenuation of Lamb waves were successfully simulated using the proposed models.

- The effects of implementing CFRP laminates to the propagation characteristics of both linear and nonlinear Lamb waves were addressed numerically and experimentally. It was found that Lamb waves experienced strong signal attenuation when wave propagating in CFRP laminates. It was also noted that Lamb waves experienced stronger dispersion in CFRP plates but the wave group velocity almost remained constant.

6.2. Recommendation for future work

This research project presents numerical and experimental studies of the interaction of fatigue crack with both linear and nonlinear Lamb waves, and proposes methodologies to monitor the fatigue crack propagation and initiation in CFRP-strengthened steel plates. However, much work still remains before employing Lamb wave-based SHM in practice. The work presented in this dissertation notes several directions for future investigations to extend the proposed methodology. The suggestions are listed below.

1) Quantitative evaluation of concealed crack initiation should be the focus of future study for CFRP-strengthened steel structures. In complex structures or civil infrastructures, fatigue crack can initiate at multiple locations simultaneously. Qualitative evaluation focusing on initiation, location and severity of one crack cannot meet the need of structural health monitoring of civil infrastructures in real-life as it may miss other defects that existed in the structure. Study of quantitative evaluation of concealed crack initiation can overcome this deficiency.
2) The proposed method should be extended to different types of defects, e.g. corrosion, surface crack and delamination. In this study, Lamb

wave-based SHM technique was only used to detect through-thickness fatigue crack. However, CFRP strengthened steel structures also suffers from corrosion, surface crack, delamination and debonding. It is essential to assess the feasibility of using proposed method to detect these types of defects to maintain the integrity of the structures.

3) The proposed method should be extended to more complex structures. In this study, the geometry of the specimen is very simple. However, in real-life, the structures are always complex. It is well-known that Lamb waves are sensitive to geometry and material changes. Hence, it is important to assess the effects of the complexity of the host structure on the propagation of Lamb waves and the ability to detect defects.
4) The attenuation and dispersion nature of damage-induced nonlinearity should be studied. In this study, it was noted that damage-induced nonlinearity strongly attenuated when propagating in CFRP laminates. Hence, it is important to study the attenuation nature of damage-induced nonlinearity. It can help future researchers to better design their sensor network and to select the excitation wave modes.

References

1. Zhao, X.-L. and L. Zhang, *State-of-the-art review on FRP strengthened steel structures.* Engineering Structures, 2007. **29**(8): p. 1808-1823.
2. Cesnik, C.E.S. and A. Raghavan, *Review of guided-wave structural health monitoring.* The Shock and Vibration Digest, 2007. **39**: p. 91+.
3. Su, Z. and L.Ye., *Identification of Damage Using Lamb Waves: From Foundamentals to Applications*, ed. P.D.-I.P.W. Prof. Dr.-Ing. Friedrich Pfeiffer. Vol. 48. 2009: Springer-Verlag Berlin Heidelberg. 355.
4. Su, Z., L. Ye, and Y. Lu, *Guided Lamb waves for identification of damage in composite structures: A review.* Journal of Sound and Vibration, 2006. **295**(3–5): p. 753-780.
5. Tang, H.-Y., et al., *Composite Structural Health Monitoring Through Use of Embedded PZT Sensors.* Journal of Intelligent Material Systems and Structures, 2011. **22**(8): p. 739-755.
6. Quaegebeur, N., P.C. Ostiguy, and P. Masson, *Correlation-based imaging technique for fatigue monitoring of riveted lap-joint structure.* Smart Materials and Structures, 2014. **23**(5): p. 055007.
7. Hong, M., et al. *Fatigue damage localization using time-domain features extracted from nonlinear Lamb waves*. 2014.
8. Kim, Y.-H., et al., *Damage assessment in layered composites using spectral analysis and Lamb wave.* Composites Part B: Engineering, 2007. **38**(7–8): p. 800-809.
9. Diamanti, K., C. Soutis, and J.M. Hodgkinson, *Piezoelectric transducer arrangement for the inspection of large composite structures.* Composites Part A: Applied Science and Manufacturing, 2007. **38**(4): p. 1121-1130.
10. Wilcox, P.D., M.J.S. Lowe, and P. Cawley, *Mode and Transducer Selection for Long Range Lamb Wave Inspection.* Journal of Intelligent Material Systems and Structures, 2001. **12**(8): p. 553-565.
11. Wang, X., Y. Lu, and J. Tang, *Damage detection using piezoelectric transducers and the Lamb wave approach: I. System analysis.* Smart Materials and Structures, 2008. **17**(2): p. 025033.
12. Cuc, A. and V. Giurgiutiu, *Embedded non-destructive evaluation for structural health monitoring, damage detection, and failure prevention.* The Shock and Vibration Digest, 2005. **37**: p. 83+.
13. Diligent, O., et al., *Reflection of the S0 Lamb Mode from a Part-Depth Circular Defect in a Plate, When the Incident Wave is Created by a Small Source.* AIP Conference Proceedings, 2003. **657**(1): p. 197-204.
14. Diligent, O., et al., *The low-frequency reflection and scattering of the S0 Lamb mode from a circular through-thickness hole in a plate: Finite Element, analytical and experimental studies.* The Journal of the Acoustical Society of America, 2002. **112**(6): p. 2589-2601.

15. Ghosh, T., T. Kundu, and P. Karpur, *Efficient use of Lamb modes for detecting defects in large plates.* Ultrasonics, 1998. **36**(7): p. 791-801.
16. Lowe, M.J.S., et al., *The low frequency reflection characteristics of the fundamental antisymmetric Lamb wave a0 from a rectangular notch in a plate.* The Journal of the Acoustical Society of America, 2002. **112**(6): p. 2612-2622.
17. Ge, M., et al., *Feature Extraction From Energy Distribution of Stamping Processes Using Wavelet Transform.* Journal of Vibration and Control, 2002. **8**(7): p. 1023-1032.
18. Sun, K., et al., *Damage Identification in Thick Steel Beam Based on Guided Ultrasonic Waves.* Journal of Intelligent Material Systems and Structures, 2010. **21**(3): p. 225-232.
19. Ihn, J.-B. and F.-K. Chang, *Detection and monitoring of hidden fatigue crack growth using a built-in piezoelectric sensor/actuator network: I. Diagnostics.* Smart Materials and Structures, 2004. **13**(3): p. 609.
20. Dai, D. and Q. He, *Structure damage localization with ultrasonic guided waves based on a time–frequency method.* Signal Processing, 2014. **96, Part A**(0): p. 21-28.
21. Ben, B.S., et al., *Damage identification in composite materials using ultrasonic based Lamb wave method.* Measurement, 2013. **46**(2): p. 904-912.
22. Pavlopoulou, S., et al. *Analysis of instantaneous characteristics of guided ultrasonic waves in metallic structures with aluminium repair patches*. 2011.
23. Liu, S., et al., *Diagnosis of structural cracks using wavelet transform and neural networks.* NDT & E International, 2013. **54**(0): p. 9-18.
24. Moll, J., et al., *Multi-site damage localization in anisotropic plate-like structures using an active guided wave structural health monitoring system.* Smart Materials and Structures, 2010. **19**(4): p. 045022.
25. Sohn, H., et al., *Nonlinear ultrasonic wave modulation for online fatigue crack detection.* Journal of Sound and Vibration, 2014. **333**(5): p. 1473-1484.
26. Ye, L., et al., *Conjunctive and compromised data fusion schemes for identification of multiple notches in an aluminium plate using lamb wave signals.* Ultrasonics, Ferroelectrics, and Frequency Control, IEEE Transactions on, 2010. **57**(9): p. 2005-2016.
27. Yan, Z., A. Miyamoto, and Z. Jiang, *Frequency slice wavelet transform for transient vibration response analysis.* Mechanical Systems and Signal Processing, 2009. **23**(5): p. 1474-1489.
28. Yan, Z., et al., *An overall theoretical description of frequency slice wavelet transform.* Mechanical Systems and Signal Processing, 2010. **24**(2): p. 491-507.

29. Cho, H. and C.J. Lissenden, *Structural health monitoring of fatigue crack growth in plate structures with ultrasonic guided waves.* Structural Health Monitoring, 2012. **11**(4): p. 393-404.
30. Lu, Y., et al., *Quantitative assessment of through-thickness crack size based on Lamb wave scattering in aluminium plates.* NDT & E International, 2008. **41**(1): p. 59-68.
31. Lu, Y., et al., *Lamb wave based monitoring of fatigue crack growth using principal component analysis*.
32. Hu, N., et al., *Characterization of damage size in metallic plates using Lamb waves.* Structural Health Monitoring, 2012. **11**(2): p. 125-137.
33. Gangadharan, R., et al., *Time reversal technique for health monitoring of metallic structure using Lamb waves.* Ultrasonics, 2009. **49**(8): p. 696-705.
34. Zhu, R., G.L. Huang, and F.G. Yuan, *Fast damage imaging using the time-reversal technique in the frequency–wavenumber domain.* Smart Materials and Structures, 2013. **22**(7): p. 075028.
35. An, J., et al., *Experimental study on identifying cracks of increasing size using ultrasonic excitation.* Structural Health Monitoring, 2012. **11**(1): p. 95-108.
36. Zhou, C., Z. Su, and L. Cheng, *Probability-based diagnostic imaging using hybrid features extracted from ultrasonic Lamb wave signals.* Smart Materials and Structures, 2011. **20**(12): p. 125005.
37. Zhou, C., Z. Su, and L. Cheng, *Quantitative evaluation of orientation-specific damage using elastic waves and probability-based diagnostic imaging.* Mechanical Systems and Signal Processing, 2011. **25**(6): p. 2135-2156.
38. Wu, Z., X.P. Qing, and F.-K. Chang, *Damage detection for composite laminate plates with a distributed hybrid PZT/FBG sensor network.* Journal of Intelligent Material Systems and Structures, 2009. **20**(9): p. 1069-1077.
39. Ihn, J.-B. and F.-K. Chang, *Pitch-catch Active Sensing Methods in Structural Health Monitoring for Aircraft Structures.* Structural Health Monitoring, 2008. **7**(1): p. 5-19.
40. Su, Z., et al., *Acousto-ultrasonics-based fatigue damage characterization: Linear versus nonlinear signal features.* Mechanical Systems and Signal Processing, 2014. **45**(1): p. 225-239.
41. Gorgin, R., Z. Wu, and Y. Zheng, *Probability-Based Diagnostic Imaging Technique Using Error Functions for Active Structural Health Monitoring.* Int. Journal of Engineering Research and Applications, 2014. **4**: p. 112-118.
42. Su, Z., et al., *Diagnostic Imaging for Structural Damage.* Advanced Materials Research, 2008. **47-50**: p. 1157-1160.

43. Wu, Z., et al., *Validation and evaluation of damage identification using probability-based diagnostic imaging on a stiffened composite panel.* Journal of Intelligent Material Systems and Structures, 2014.
44. Chen, D., et al., *Assessment of Urban Heat Island and Mitigation by Urban Green Coverage*, in *Mitigating Climate Change*, A. Khare and T. Beckman, Editors. 2013, Springer Berlin Heidelberg. p. 247-257.
45. He, J., et al., *A multi-feature integration method for fatigue crack detection and crack length estimation in riveted lap joints using Lamb waves.* Smart Materials and Structures, 2013. **22**(10): p. 105007.
46. Jhang, K-Y., *Applications of nonlinear ultrasonics to the NDE of material degradation.* Ultrasonics, Ferroelectrics, and Frequency Control, IEEE Transactions on, 2000. **47**(3): p. 540-548.
47. Deng, M. and J. Pei, *Assessment of accumulated fatigue damage in solid plates using nonlinear Lamb wave approach.* Applied Physics Letters, 2007. **90**(12): p. 121902.
48. Deng, M., *Cumulative second-harmonic generation of Lamb-mode propagation in a solid plate.* Journal of Applied Physics, 1999. **85**(6): p. 3051-3058.
49. Chao, Z., et al., *Evaluation of fatigue cracks using nonlinearities of acousto-ultrasonic waves acquired by an active sensor network.* Smart Materials and Structures, 2013. **22**(1): p. 015018.
50. Christoph, P., et al., *Evaluation of fatigue damage using nonlinear guided waves.* Smart Materials and Structures, 2009. **18**(3): p. 035003.
51. Hong, M., et al., *Locating fatigue damage using temporal signal features of nonlinear Lamb waves.* Mechanical Systems and Signal Processing, 2015. **60–61**: p. 182-197.
52. Hong, M., et al., *Modeling nonlinearities of ultrasonic waves for fatigue damage characterization: Theory, simulation, and experimental validation.* Ultrasonics, 2014. **54**(3): p. 770-778.
53. Kawashima, K., et al., *Nonlinear acoustic response through minute surface cracks: FEM simulation and experimentation.* Ultrasonics, 2002. **40**(1–8): p. 611-615.
54. Dutta, D., et al., *A nonlinear acoustic technique for crack detection in metallic structures.* Structural Health Monitoring, 2009. **8**(3): p. 251-262.
55. Palit Sagar, S., et al., *Non-linear ultrasonic technique to assess fatigue damage in structural steel.* Scripta Materialia, 2006. **55**(2): p. 199-202.
56. Chillara, V.K. and C.J. Lissenden, *Review of nonlinear ultrasonic guided wave nondestructive evaluation: theory, numerics, and experiments.* Optical Engineering, 2015. **55**(1): p. 011002-011002.
57. Jhang, K.-Y., *Nonlinear ultrasonic techniques for nondestructive assessment of micro damage in material: A review.* International Journal of Precision Engineering and Manufacturing, 2009. **10**(1): p. 123-135.

58. Lee, T.-H., I.-H. Choi, and K.-Y. Jhang, *The nonlinearity of guided wave in an elastic plate.* Modern Physics Letters B, 2008. **22**(11): p. 1135-1140.
59. de Lima, W.J.N. and M.F. Hamilton, *Finite-amplitude waves in isotropic elastic plates.* Journal of Sound and Vibration, 2003. **265**(4): p. 819-839.
60. Jiao, J.-P., et al., *Nonlinear Acoustic Interaction of Contact Interfaces.* Experimental Mechanics, 2013. **54**(1): p. 63-68.
61. Hirose, S. and J.D. Achenbach, *Higher harmonics in the far field due to dynamic crack-face contacting.* The Journal of the Acoustical Society of America, 1993. **93**(1): p. 142-147.
62. Solodov, I.Y., *Ultrasonics of non-linear contacts: propagation, reflection and NDE-applications.* Ultrasonics, 1998. **36**(1–5): p. 383-390.
63. Donskoy, D., A. Sutin, and A. Ekimov, *Nonlinear acoustic interaction on contact interfaces and its use for nondestructive testing.* NDT & E International, 2001. **34**(4): p. 231-238.
64. Pecorari, C., *Nonlinear interaction of plane ultrasonic waves with an interface between rough surfaces in contact.* The Journal of the Acoustical Society of America, 2003. **113**(6): p. 3065-3072.
65. Kim, J.Y., A. Baltazar, and S.I. Rokhlin, *Ultrasonic assessment of rough surface contact between solids from elastoplastic loading–unloading hysteresis cycle.* Journal of the Mechanics and Physics of Solids, 2004. **52**(8): p. 1911-1934.
66. Giurgiutiu, V. and J. Bao, *Embedded-ultrasonics Structural Radar for In Situ Structural Health Monitoring of Thin-wall Structures.* Structural Health Monitoring, 2004. **3**(2): p. 121-140.
67. Yu, Q.-Q., et al., *Tests on Cracked Steel Plates with Different Damage Levels Strengthened by CFRP Laminates.* International Journal of Structural Stability and Dynamics, 2014. **14**(06): p. 1450018.
68. Wu, C., et al., *Fatigue tests on steel plates with longitudinal weld attachment strengthened by ultra high modulus carbon fibre reinforced polymer plate.* Fatigue & Fracture of Engineering Materials & Structures, 2013. **36**(10): p. 1027-1038.
69. Lowe, M. and B. Pavlakovic., *Disperse*. 2013, Imperial College: London.
70. Dong, W., et al., *A damage diagnostic imaging algorithm based on the quantitative comparison of Lamb wave signals.* Smart Materials and Structures, 2010. **19**(6): p. 065008.
71. Lee, B.C. and W.J. Staszewski, *Modelling of Lamb waves for damage detection in metallic structures: Part I. Wave propagation.* Smart Materials and Structures, 2003. **12**(5): p. 804.
72. Rose, J.L. and J.L. Rose, *Finite Element Method for Guided Wave Mechanics Ultrasonic Guided Waves in Solid Media*. 2014: Cambridge University Press.

Appendix

Conference paper

1. Wang, Y., Y. Lu, W. Duan and X-L. Zhao, Monitoring Crack Propagation in Carbon-Fibre-Reinforced-Polymer- Strengthened Steel Plates Using Lamb Waves, SHMII-07: *7th International Conference on Structural Health Monitoring of Intelligent Infrastructure*, July 1-3, 2015, Torino, Italy

Journal paper

1. Wang, Y., Y. Lu and W. Duan, Detection of fatigue crack initiation in Fibre-Reinforced-Polymer (FRP) Strengthened Steel Plate Using nonlinear Lamb Waves, (*prepare to submit*)